Latent heat recovery from a counterflow direct contact falling droplet heat exchanger
by Stephen Edward Izbicki

A thesis submitted in partial fulfillment of the requirements for the degree of Master of Science in Mechanical Engineering
Montana State University

Abstract:
Heat recovery in one configuration of a direct contact counterflow, falling droplet heat exchanger (DCHX), from natural gas combustion products was evaluated in terms of sensible and latent effectiveness. Effectiveness was found for uniform and nonuniform water droplet streams, and high and low inlet gas humidity ratios over a range of droplet flow rates and inlet gas temperatures. A droplet generator was built and tested to characterize droplet uniformity under various operating conditions. Uniform droplets were produced by vibrating the droplet generator at a fixed frequency and amplitude. Results agree well with those predicted by Rayleigh's theory on the instability of liquid jets. A stream of nonuniform drops, having standard deviations two to four times higher than the uniform stream, was produced when the generator was not vibrated. Preliminary heat exchange studies show single phase energy and two phase mass balances within about 6 %, indicating reasonable accuracy of temperature and flow measuring apparatus. DCHS effectiveness, defined in sensible heat recovery terms, is. shown to be further from its thermodynamic limit than that of a standard (no direct contact) counterflow heat exchanger in the same range of NTU values. A modified effectiveness is defined which includes the latent heat availability of the inlet gas stream. Modified effectiveness values were about 50% of their sensible counterparts indicating that latent heat recovery could be significantly improved.

LATENT HEAT RECOVERY FROM A COUNTERFLOW DIRECT CONTACT FALLING DROPLET HEAT EXCHANGER

by

Stephen Edward Izbicki

A thesis submitted in partial fulfillment
of the requirements for the degree

of

Master of Science

in

Mechanical Engineering

MONTANA STATE UNIVERSITY
Bozeman, Montana

June 1986

APPROVAL

of a thesis submitted by

Stephen Edward Izbicki

This thesis has been read by each member of the thesis committee and has been found to be satisfactory regarding content, English usage, format, citations, bibliographic style, and consistency, and is ready for submission to the College of Graduate Studies.

6/5/86
Date

Thomas G. Dierkhorn
Chairperson, Graduate Committee

Approved for the Major Department

6-5-86
Date

Michael Ghall
Head, Major Department

Approved for the College of Graduate Studies

8/22/86
Date

Henry L. Parsons
Graduate Dean

STATEMENT OF PERMISSION TO USE

In presenting this thesis in partial fulfillment of the requirements for a master's degree at Montana State University, I agree that the Library shall make it available to borrowers under rules of the Library. Brief quotations from this thesis are allowable without special permission, provided that accurate acknowledgement of source is made.

Permission for extensive quotation from reproduction of this thesis may be granted by my major professor, or in his absence, by the Director of Libraries when, in the opinion of either, the proposed use of the material is for scholarly purposes. Any copying or use of the material in this thesis for financial gain shall not be allowed without my written permission.

Stephen E. Gyberich
Signature

8-9-86
Date

ACKNOWLEDGEMENT

The author is indebted to Dr. Thomas Reihman for his guidance throughout this investigation. Special thanks to Dr. Anthony Demetriades for his suggestions and encouragement. Thanks also to Dr. William Martindale for his support as a committee member.

This study was funded by the Department of Mechanical Engineering and the Engineering Experiment Station of Montana State University.

TABLE OF CONTENTS

LIST OF TABLES

LIST OF FIGURES

NOMENCLATURE

Symbol	Description
C_D	drag coefficient
C_p	specific heat, kJ/kg-°K
C_R	thermal capacitance ratio
C_d, C_∞	droplet, freestream mass concentration, kg/m³
D_{AB}	mass diffusivity, m²/s
D_d	droplet diameter, mm
d_j, d_t	jet, tube diameter, mm
F	vibration frequency, Hz
g	gravitational acceleration, m/s²
h_{fg}	latent heat of vaporization, kJ/kg
h_c, h_d	thermal, diffusion convective coefficient, W/m²-°K
k	thermal conductivity, W/m-°K
L	column length, m
NTU	number of transfer units
M_L, M_{dg}	liquid, dry gas molecular weight, kg/kg-mole
$\mathring{m}, \mathring{m}_{dg}$	wet, dry gas mass flow rate, kg/s
P_v	vapor pressure, kPa
q	heat transfer rate, W
R	thermal resistance, °K/W
T	temperature, °K
t_c, t_R	droplet contact, residence time, s
V	velocity, cm/s

NOMENCLATURE--continued

Symbol	Description
Greek Letters	
δ	surface tension, N/m
$\varepsilon_s, \varepsilon_L$	sensible, latent effectiveness
λ	wavelength, mm
μ	dynamic viscosity, kg/m-s
v	kinematic viscosity, m^2/s
ρ	mass density, kg/m^3
σ	standard deviation
ω	gas humidity ratio, kg_L/kg_{dg}
Non Dimensional Parameters	
Bi	Biot number, $h_c L_c / k_d$
Le	Lewis number, $k_g/(\rho C_p)_g D_{AB}$
Nu	Nusselt number, $h_c L_c / k_g$
Pr	Prandtl number, $C_p \mu / k_g$
Re	Reynolds number, $V L_c / v$
Sc	Schmidt number, $\mu / \rho D_{AB}$
Sh	Sherwood number, $h_d L_c / D_{AB}$
Subscripts	
1	DCHX inlet
2	DCHX outlet
d	droplet
dg	dry gas
g	gas
in	test section inlet

NOMENCLATURE--Continued

Symbol	Description
j	jet
L	liquid
lm	log mean
m	measured
min	minimum
nc	natural convection
opt	optimum
out	test section exit
p	predicted
r	radiative
s	inner surface
T	terminal
tot	total
∞	freestream conditions

ABSTRACT

Heat recovery in one configuration of a direct contact counterflow, falling droplet heat exchanger (DCHX), from natural gas combustion products was evaluated in terms of sensible and latent effectiveness. Effectiveness was found for uniform and nonuniform water droplet streams, and high and low inlet gas humidity ratios over a range of droplet flow rates and inlet gas temperatures . A droplet generator was built and tested to characterize droplet uniformity under various operating conditions. Uniform droplets were produced by vibrating the droplet generator at a fixed frequency and amplitude. Results agree well with those predicted by Rayleigh's theory on the instability of liquid jets. A stream of nonuniform drops, having standard deviations two to four times higher than the uniform stream, was produced when the generator was not vibrated. Preliminary heat exchange studies show single phase energy and two phase mass balances within about 6%, indicating reasonable accuracy of temperature and flow measuring apparatus. DCHX effectiveness, defined in sensible heat recovery terms, is shown to be further from its thermodynamic limit than that of a standard (no direct contact) counterflow heat exchanger in the same range of NTU values. A modified effectiveness is defined which includes the latent heat availability of the inlet gas stream. Modified effectiveness values were about 50% of their sensible counterparts indicating that latent heat recovery could be significantly improved.

CHAPTER I

INTRODUCTION

Substantial amounts of low temperature energy, with the potential to reduce fuel consumption, are being lost through combustion gas exhaust streams. Examples of such situations are industrial boilers, gas turbine exhausts, domestic hot water heaters and wood stoves. As fuel costs escalate and its availability decreases, the need for technology to recover this wasted energy will become increasingly more important. Existing recovery methods consider minimum flue gas exit temperatures to be 400-420°K. This temperature is usually limited by the need to avoid forming acidic condensate in the heat exchanger.[1,2]

Direct contact heat exchangers (DCHX) afford several advantages over conventional types. For conventional heat exchangers, the intermediate heat exchange surfaces increase thermal resistance thereby decreasing system efficiency. In addition, these surfaces are prone to corrosion and scaling which further increases thermal resistance and requires maintenance. Since the DCHX has no such surface these problems do not exist. It is estimated that heat transfer coefficients ten times higher are possible using a DCHX in favor of conventional types.[3]

This geometry is also known to be effective in removing

particulate and certain water soluble gases from combustion product emissions. Fine particle collection, whose efficiency is strongly influenced by droplet Reynolds number, can be achieved with drop diameters up to .5mm falling at their terminal velocity [4]. Water soluble pollutant gases such as SO_2, NO_2 and H_2S can be removed by absorption. The driving force for this mechanism is the difference between the partial pressure of the soluble gas (pollutant) in the gas mixture and the vapor pressure of the solute gas (pollutant) in the liquid.[5] This difference is favorable for SO_2 absorbtion and moderately favorable for NO_2 and H_2S. It is assumed that in a commercially useable unit, the DCHX will be a closed system with a secondary heat exchanger. This configuration will require a filter or other purification device in the DCHX loop to remove acid and particulate buildup from the working fluid.

Although direct contact heat exchange has long been used in industry, specific data pertaining to performance is limited. Fair [6] reviews works on analysis and design of industrial DCHX's. He presents heat transfer correlations for spray column heat exchangers using hollow and solid cone spray nozzles. Drop sizes delivered from these nozzles typically vary over a wide range since they are designed to provide uniform application, not uniform drop size. Sideman and Moalem-Maron [7] examined over one hundred works published from 1922 to 1979 on condensation heat exchangers. Of the seven publications cited for dealing with droplet

formity. Goren and Wilke [8] used uniformly sized Aroclor drops on which to condense steam. More recently , Sekins and Thayer [9] report heat exchanger effectiveness of around 48% for 1mm monodisperse silicon oil drops in airflow. They comment that natural breakup(no imposed oscillations) results in a wide range of small and large drops [10]. None of the above studies however, show how drop size variation influences DCHX effectiveness. Mussulman and Warrington [11] have written a computer model which shows, for a mean droplet size of 2.1mm, that reducing the size distribution from 50% to 5% increased the effectiveness of an air cooling tower by 100%.

The aim of the present study is to determine the influence changes in droplet monodispersity have on DCHX effectiveness over a range of operating conditions. It is proposed that a monodisperse droplet stream maximizes heat transfer for this configuration. Heat exchange is enhanced by the large number of small drops, increasing heat transfer surface area for a given water flow rate. For a fixed DCHX column diameter, the optimum gas flow rate is determined by the terminal velocity of the smallest drop. If this were not the case, the smallest drops would be carried out of the DCHX column by the gas stream, leading to makeup water requirements. Minimum column length is a function of droplet residence time. Large drops have comparatively low surface area to volume ratios, high Biot numbers and high terminal velocities. As a result, large drops have higher

terminal velocities. As a result, large drops have higher residence times, lower contact times and lower overall heat transfer rates than smaller drops. Consequently narrowing the drop size dispersion should improve effectiveness.

The present study was carried out in two parts. First a monodisperse droplet generator was tested to characterize the size dispersion of droplets produced under various operating conditions. Next the effectiveness of a vertical tube heat exchanger, utilizing the droplet generator, was evaluated. In this configuration, a monodisperse stream of falling water droplets extracts energy from a counterflow of natural gas combustion products (see figure 1). As mentioned previously, a commercially useable unit will most likely be a closed system. However for simplicity's sake, the present DCHX system is an open one. It is shown that a nearly monodisperse droplet stream (σ=5%) can be produced by mechanically disturbing, at a specified frequency, a plate to which a group of equally spaced capillary tubes, producing jets, are attached. Conversely, a randomly sized droplet stream (σ=10-20%) will result if this disturbance is removed. Heat exchanger effectiveness was determined for the DCHX over a range of operating conditions, for uniform and nonuniform droplets, and for air and natural gas combustion products.

In light of the above discussion, it seemed logical to organize this paper in a similar manner. Therefore the remaining discussion is comprised of three parts. Chapter

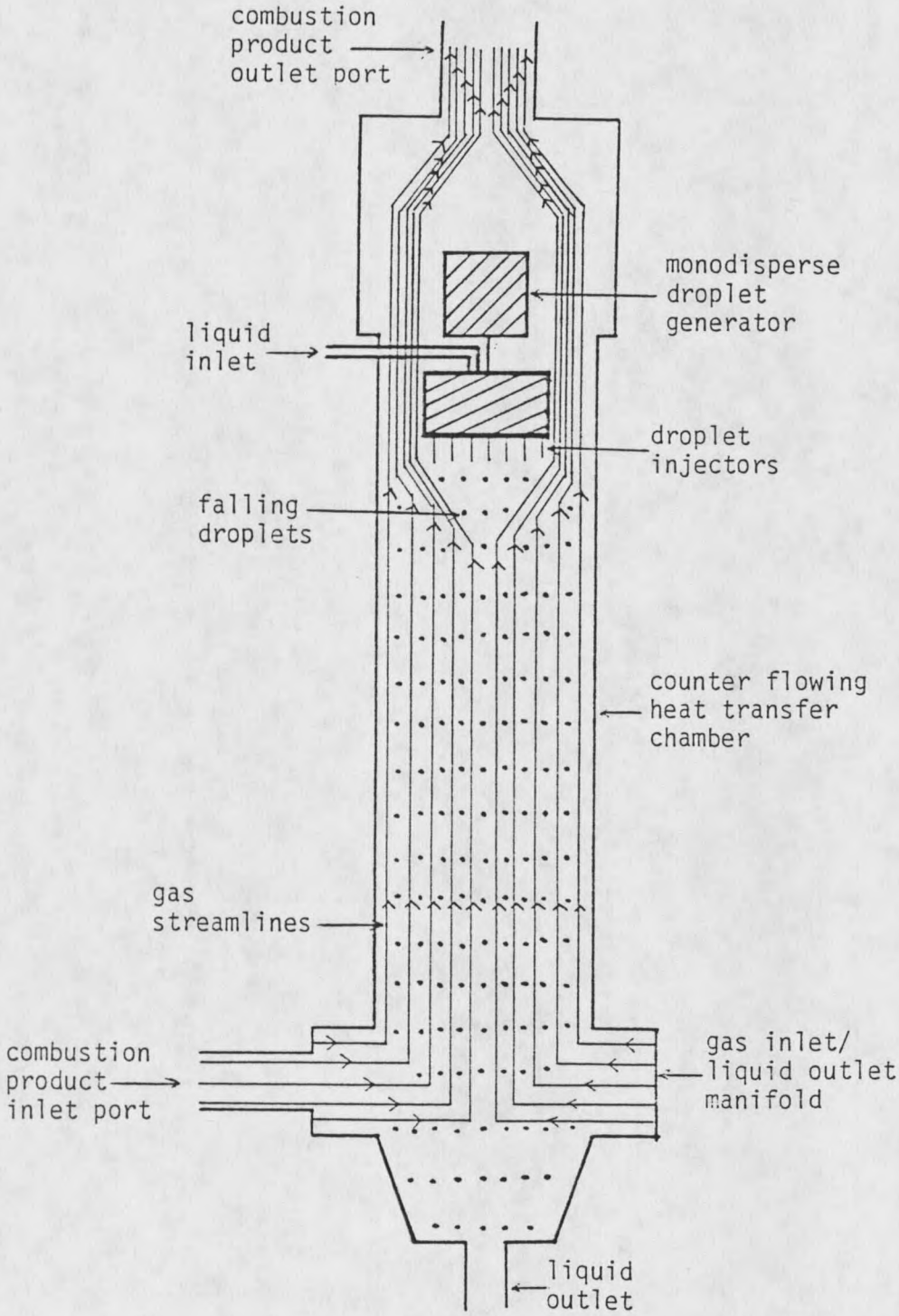

Figure 1: Simplified Sketch of a Falling Droplet DCHX

II describes techniques used in producing and measuring a monodisperse droplet stream. This includes a report of current uniform droplet production theory and the results of droplet characterization studies. In Chapter III, results from the first study are used as the basis for variations in drop size dispersion in the DCHX performance experiments. DCHX experimental apparatus and procedure are reviewed in Chapter III, along with development of the theoretical background and a discussion of pertinent results. The conclusions section, Chapter IV, is concerned with results from both the monodisperse droplet and DCHX performance studies.

CHAPTER II

MONODISPERSE DROPLET STUDY

Background

It is of critical importance in the current investigation to show that a water droplet stream of nearly uniform size and spacing is produced by axially vibrating a capillary jet. This phenomenon is well documented in the literature. Devices used to produce such a stream in this manner are based on Rayleigh's analysis on the instability of capillary jets [12] for an inviscid liquid. Rayleigh showed that the frequency of vibration which leads most rapidly to the disintegration of a liquid column is given by:

$$F_{opt}=V_j/4.508d_j \qquad (2.01)$$

Rajagopalon and Tien [13] have shown that uniformly sized drops are produced over a frequency range in which column wavelength λ, varies between $3.5d_j$ and $6.5d_j$. These limits correspond closely to those found experimentally ($3.5d_j<\lambda<7d_j$) by Schneider and Hendricks [14]. Rayleigh's linearized theory predicts that the lower limit should be $\lambda_{min}=(\pi)d_j$ [9].

Linblad and Schneider [15] report that, in order to overcome viscous forces, capillary jets must have a minimum velocity to be established. This minimum is a function of liquid density, surface tension, and jet diameter. It is

given by:

$$(V_{j,min})^2 = 8\delta/\rho_d d_j \qquad (2.02)$$

However Dabora [16] has found actual minimum velocities up to 35% lower than equation (2.02) predicts.

By conservation of mass, the volume of one drop equals the volume of a water column one wavelength long, from which the ratio of drop to jet diameter is found as:

$$D_d/d_j = 1.145(V_j/Fd_j)^{1/3} \qquad (2.03)$$

Results by Rajagopalon and Tien [13] showed agreement to within 3% of equation (2.03), indicating good drop uniformity with little waste due to satellite formation.

Several authors indicate that vena contracta effects at the tube exit cause jet diameters to be somewhat less than tube diameters [15,17]. Harmon [18] assumes a laminar jet velocity distribution, and by conservation of momentum determines that $d_j = .866 d_t$. A study by Goren and Wronski [19] indicates that, for a parabolic velocity profile, jet diameter actually increases at low Reynolds numbers ($Re_j < 17$). At higher Reynolds numbers ($17 < Re_j < 100$) this diameter decreases monotonically to a value slightly higher than that which Harmon predicts ($d_j/d_t = .885$). Their analysis does not however, include viscous dissipation effects. They suggest that at sufficiently high jet velocities, viscous effects cause a flatter profile, and drive the ratio d_j/d_t toward unity. Schneider and Hendricks [14] and Dabora [16] have assumed this ratio to be unity in their investigations.

Mathematical formulations describing the production of

nonuniformly sized drops are sparse. Levich [20] derives an expression showing drop size, without imposed oscillations, to be of the order $D_d \sim D_{d,opt}$. $D_{d,opt}$ refers to droplets produced at the vibration frequency for maximum jet instability predicted in Rayleigh's analysis. Most of the previously cited works confirm that nonuniform droplets are produced in the absence of oscillations. They do not however, attempt to characterize the degree of nonuniformity.

Apparatus

The first step in conducting this investigation was to develop a droplet generator along with instrumentation to characterize droplet formation (see Figure 2 for schematic). Liquid at constant temperature, pressure and flow rate is delivered to the generator chamber in the following manner. Water from an isothermal source is supplied to the constant head reservoir (Figure 2) at a flow rate slightly higher than that passing through the generator chamber. Excess water is drained through the overflow outlet, providing a source of water to the capillary jets having a constant head and the proper flow rate. Jet velocities were varied by adjusting the reservoir elevation. The water source is then filtered and its temperature, flow rate and pressure are monitored immediately prior to entering the generator chamber. An oscillator-amplifier combination supplies a signal of set frequency and amplitude to the chamber by means of an MB Electronics PM500 Vibramate Excitor. Diagnostics to

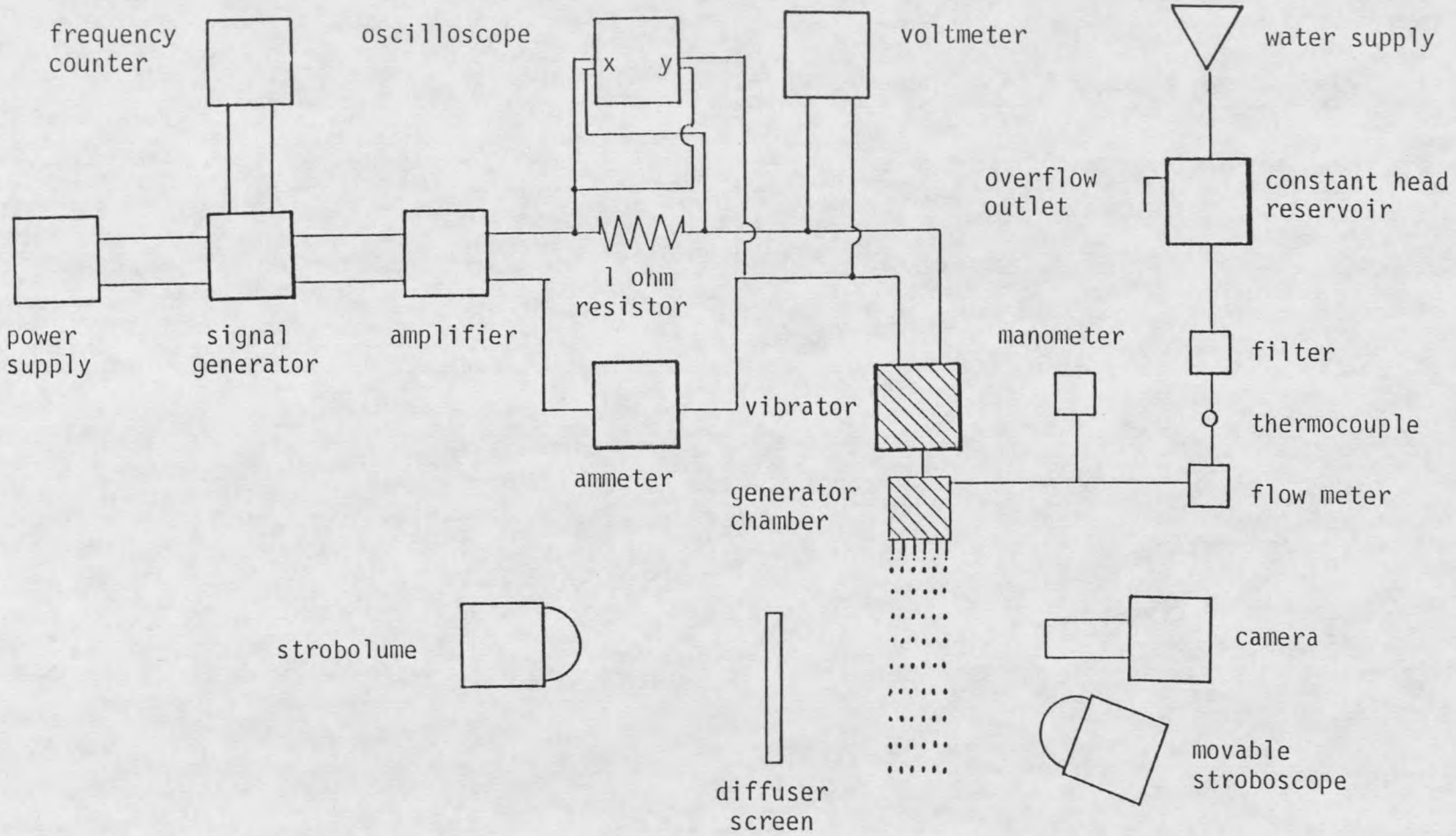

Figure 2: Schematic of Droplet Generator Power and Liquid Delivery Subsystems and Photographic Diagnostics

monitor signal frequency and power consumption are included.

The generator itself (Figure 3) is a cylindrical aluminum chamber (9.5cm i.d.x2.2cm long) fitted on the bottom with an aluminum plate (.3cm thick) drilled to accommodate a set of equally spaced stainless steel capillary tubes. All tubes were carefully machined and polished to ensure that no burrs or other irregularities were present at the ends. Each tube was inspected microscopically to show that all were sized and finished uniformly. The required inside orifice diameter was achieved by epoxying capillary jets (28mm i.d.x.47mm o.d.x23mm long) inside 13mm lengths of .47mm i.d. tubing. These were in turn epoxied into the bottom plate. Nineteen jets were used in all for these studies.

Droplet size instrumentation consisted of a 35mm Lietz-Wetzlar camera body and a Summicron 50mm f/2.0 lens fitted with a 90mm bellows. Image magnification was approximately 2:1. The camera shutter was synchronized with a General Radio 1532A Strobolume (15 μs flash duration) flash source. Photographs were taken with Kodak Plus-X-Pan film (ASA 125) using backlighting. The droplet stream fell between the camera and a 6.4mm thick translucent acrylic sheet through which the flash source was diffused. For visual observation of the stream a General Radio 1531AB Strobotac was used to 'stop' the droplet motion by setting the Strobotac frequency to that of the excitation frequency. In each negative a stainless steel tube of known diameter appeared for size reference, coplanar with the droplet stream. Drops were

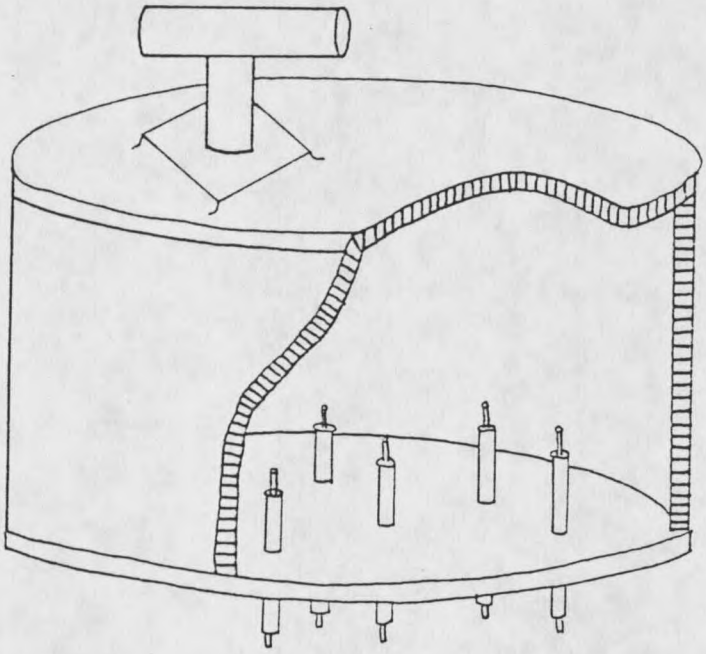

Figure 3: Droplet Generating Chamber

measured from the negatives with a Bausch and Lomb (.7x-3x) stereo measuring microscope.

Experimental Procedure

In characterizing droplet formation, the procedure has been first to determine the operating conditions for the droplet generator during DCHX tests. Next was to devise a data grid prescribing parameter variations away from the DCHX operating conditions. The parameters defining the data grid (jet velocity, vibration frequency and input power) were varied individually 15 to 40 percent above and below a data center case. The data center case corresponds to the optimum droplet operating conditions predicted for the DCHX studies in Chapter III. For example, holding jet velocity and vibration power constant at data center conditions, vibration frequency was varied from 20% below to 20% above its data center. Photographs were taken at each point on the data grid for all jets. Information on droplet formation in the absence of forced vibration was obtained for several jets over a range of velocities. In this manner, droplet uniformity at the data center, and the influence of the above parameters was determined.

Before photographing, tubes were ultrasonically cleaned, the constant head reservoir adjusted and jet velocity determined from mass flow data. Next a predetermined vibration frequency and amplitude were imposed, power consumption data recorded, and droplet motion 'stopped' using

the Strobotac. Jet disintegration was then visually inspected to insure the droplet stream fell within the camera's depth of field. A series of three photographs were then taken at this operating condition. At this point one parameter was varied and the process repeated. After development, the negatives were inspected. Of the three negatives taken at each operating condition, only those with the sharpest boundaries, showing a minimum of three droplets per frame were used. Drop measurements came directly from these negatives.

To find actual drop size, developed drop size and magnification ratio had to be known. The magnification ratio is the ratio of developed to actual size of the known diameter stainless steel tube in the negative. Droplet diameter is the average of the major and minor axes dimensions. The given drop size variation is the standard deviation (σ) for all droplets measured (three drops per photograph) for all jets measured (maximum of nineteen) at a specified operating condition.

Results and Discussion

The purpose of this study was twofold. The first concerned showing that a nearly uniform droplet stream was produced by the droplet generator described earlier, at the operating conditions (jet velocities and vibration frequency and power) used in the DCHX studies of Chapter III. It was also important to determine the sensitivity of droplet dia-

meter to changes in vibration frequency and power. Comparison of experimentally determined uniform droplet diameters are made to the theoretical prediction derived earlier.

Since it is proposed that a uniform droplet stream is the most efficient method of heat extraction for the DCHX, the other goal of this particular investigation was to find the degree to which droplets become nonuniform when emanating from a nonvibrating jet. Results are presented as percent standard deviation from the mean, over the range of jet velocities used in the DCHX studies.

Uniform Droplets

The dependence of droplet size and spacing on jet velocity is shown in Figures 4 and 5. The four droplet streams pictured in Figure 4 indicate qualitatively how, at a fixed vibration amplitude and frequency, droplet diameter and spacing increase with increasing jet velocity. Good agreement between equation (2.03) and experimentally determined drop size, plotted as a function of jet velocity, is shown in Figure 5. It is apparent in examining this figure, that although theoretical and experimental values lie within 6% of one another, a systematic error causes all experimental values to lie above their theoretical counterparts. This systematic error may be introduced by uncertainty in calculating the magnification ratio for droplet measurements. Determination of the magnification ratio requires knowing the reference tube's actual size, the microscope's

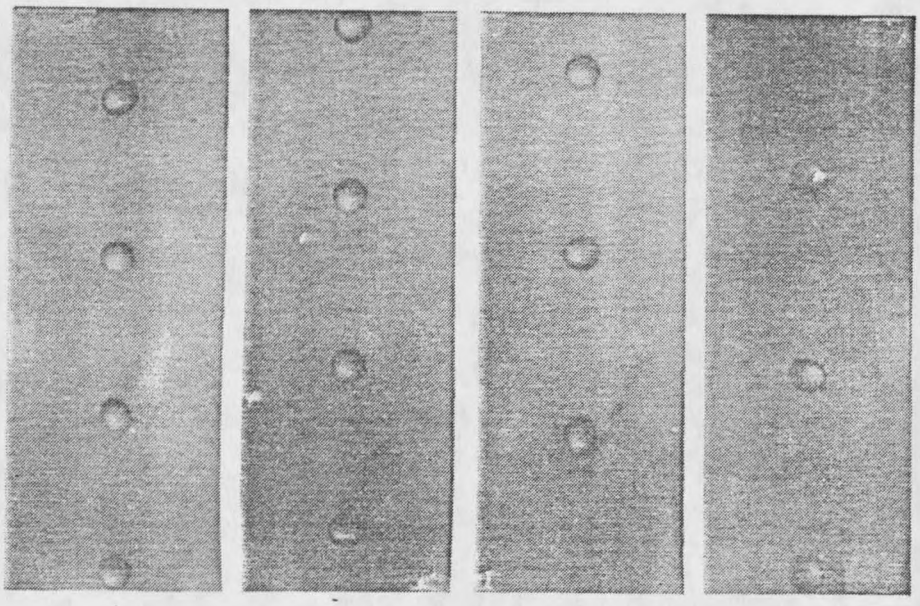

V_j=1.35m/s V_j=1.50m/s V_j=1.65m/s V_j=1.80m/s
Vibration Frequency = 850 Hz
Input Power = 1.5 W

Figure 4: Droplet Diameter vs. Jet Velocity
(Magnification Ratio - 7:1)

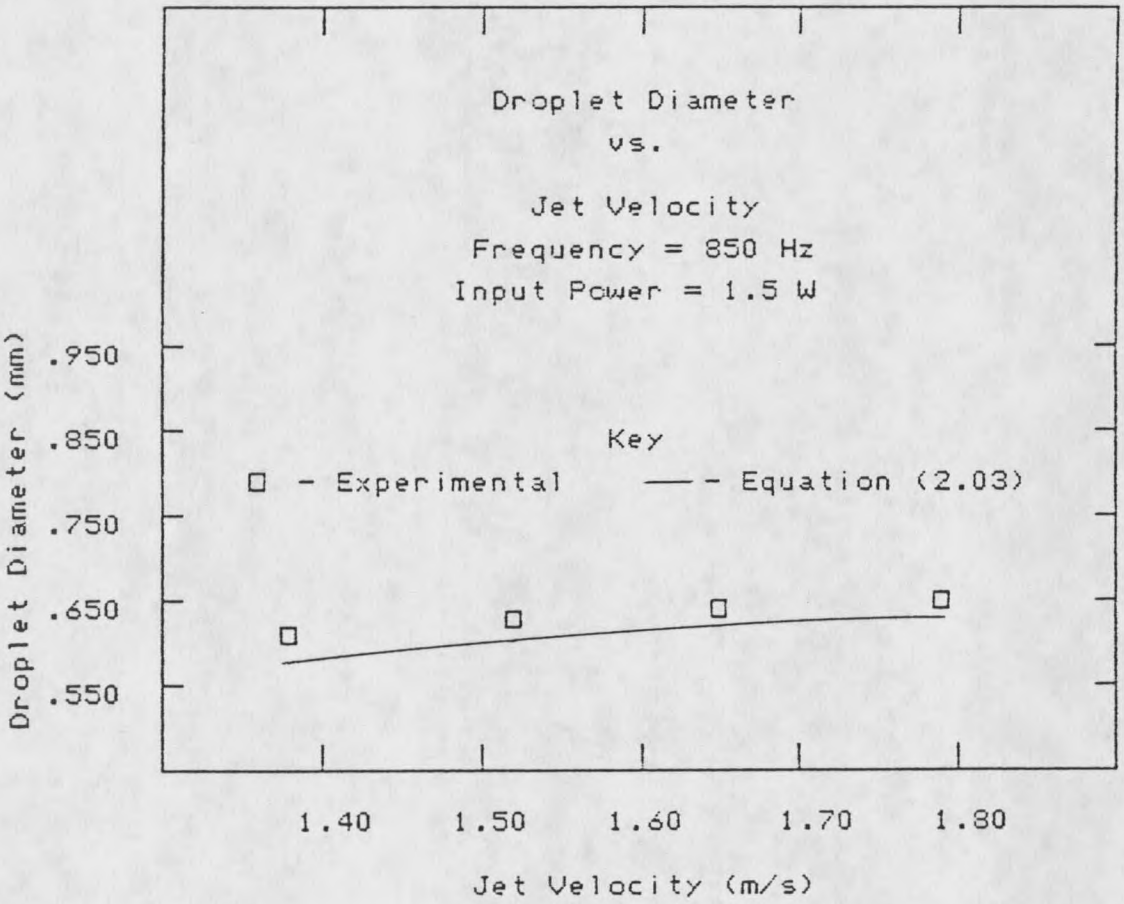

Figure 5: Theoretical and Experimental Droplet Diameter vs. Jet Velocity

magnification ratio and the photographed size of the reference tube. Actual tube size and microscope magnification ratio were constant throughout the study and known to within about 2%. Uncertainty in measuring the photographed tube size was around 4%, due to the slight 'fuzziness' of the tube boundaries on the negatives. Therefore typical uncertainties encountered in measuring the above quantities readily leads to a systematic error of the magnitude exhibited in Figure 5.

The sensitivity of droplet diameter to vibration frequency is indicated in Figure 6. Since diameter is inversely proportional to the cube root of frequency, it is only slightly sensitive to frequency changes, as is evidenced in the figure. Figure 7 shows the relation between drop diameter and vibration input power. As might be expected, droplet diameter is independent of power, at least for the range covered in this study.

Nonuniform Droplets

The nonuniformity exhibited by droplets when forced through a nonvibrating capillary jet is depicted in Figure 8. Four droplet streams, two emanating from vibrating jets and two from nonvibrating jets, all with equal jet velocities are shown. It is seen in Table 1, that the standard deviation of drops produced by nonvibrating jets is from two to four times higher than those under induced vibration.

Also included in the table is the sample mean or aver-

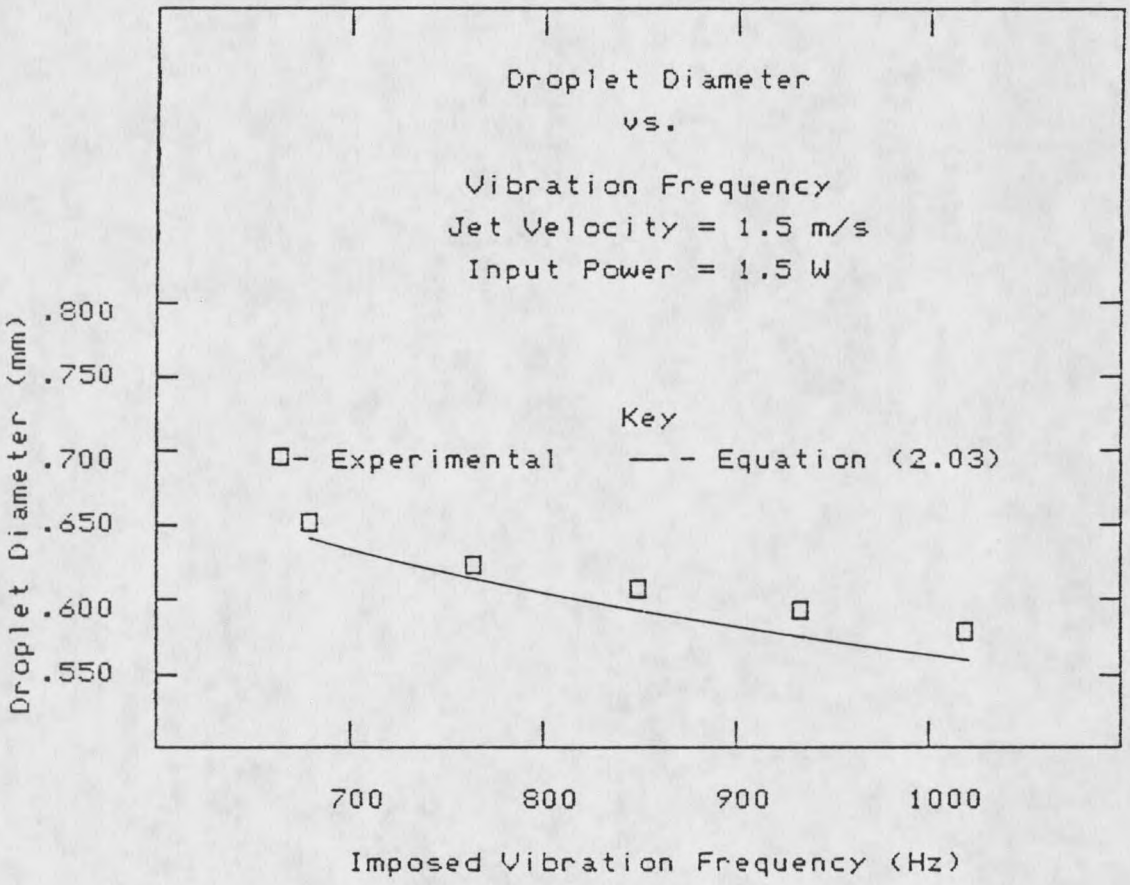

Figure 6: Theoretical and Experimental Droplet Diameter vs. Vibration Frequency

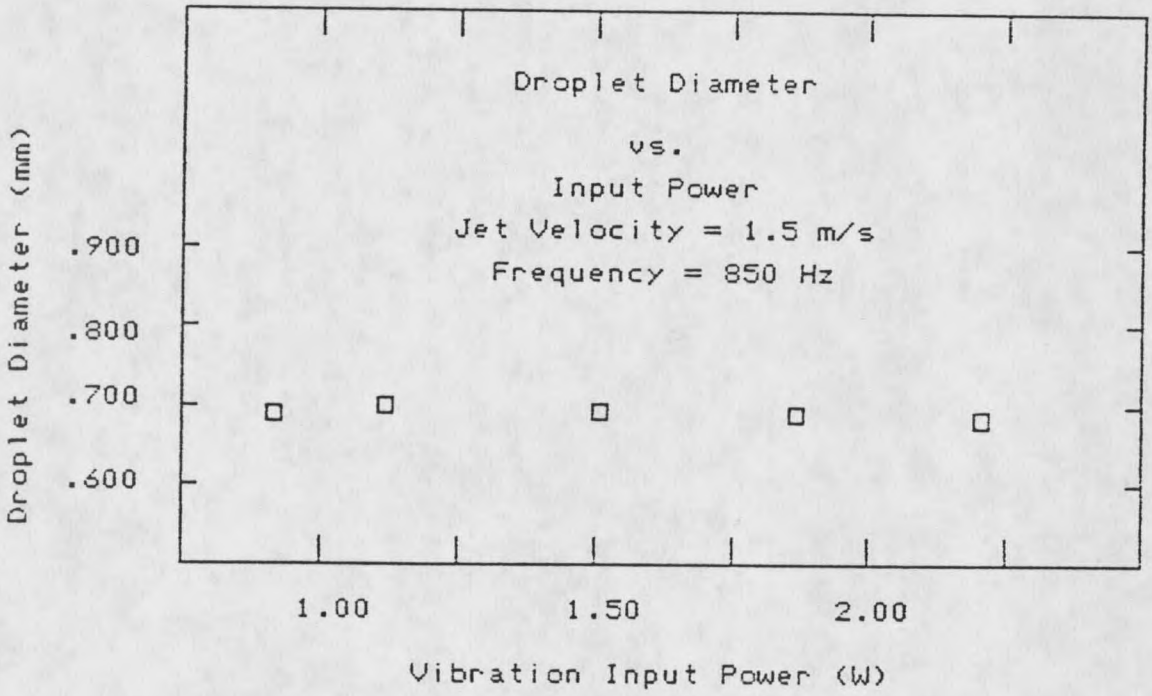

Figure 7: Experimentally Determined Droplet Diameter vs. Input Power

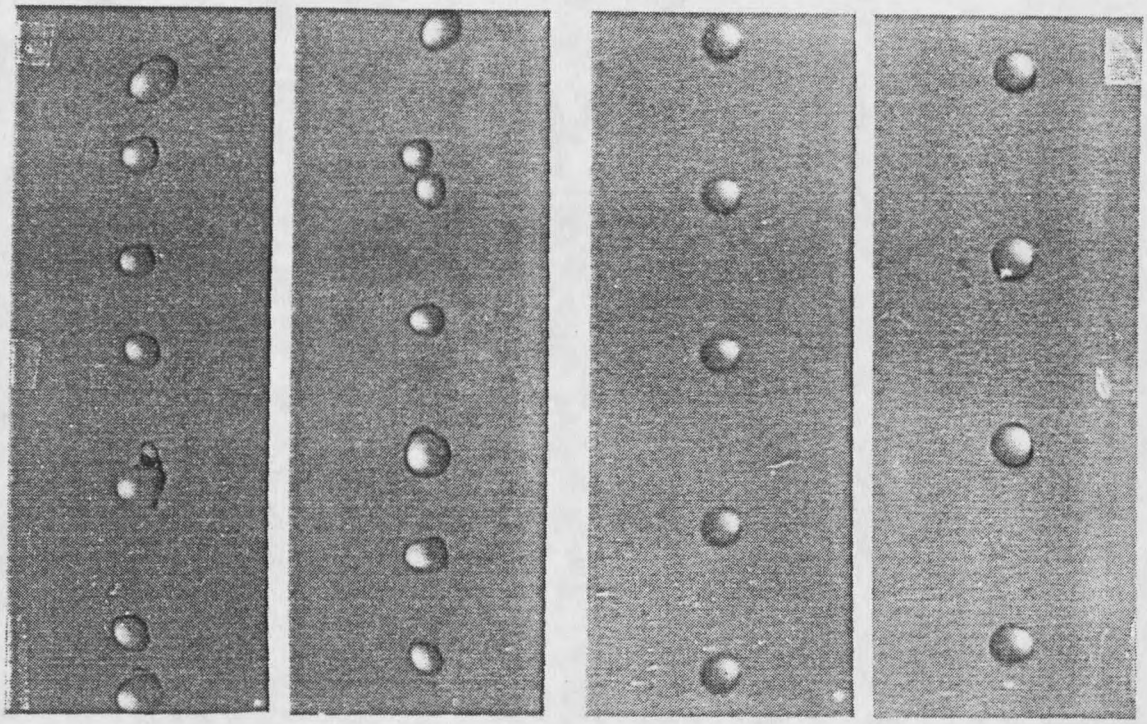

V_j=1.5 m/s F=0 Hz | V_j=1.5 m/s F=0 Hx | V_j=1.5 m/s F=935 Hz | V_j=1.5 m/s F=850 Hz

Figure 8: Droplet Size Dispersion for Vibrating and Non Vibrating Capillary Jets (Magnification Ratio - 8:1)

Table 1: Droplet Diameter Standard Deviation for Vibrating and Non Vibrating Capillary Jets

	Non Vibrating			Vibrating		
V_j (m/s)	D_{mean} (mm)	D_{mode} (mm)	σ (%)	D_{mean} (mm)	D_{mode} (mm)	σ (%)
1.77	.49	.47	13	.65	.65	5.5
1.63	.49	.45	11	.64	.64	5.1
1.47	.53	.45	20	.62	.62	5.5
1.31	.56	.48	17	.61	.61	4.8

age droplet diameter and sample mode or the most frequently occurring diameter for each sample population. These are included to show that nonuniform droplets exhibit a skewed rather than normal size distribution. For normally distributed samples, the mean and mode are equal. Samples for which the mean and mode are not equal are said to have a skewed distribution. This is important since it indicates that the larger standard deviations shown by the nonvibrating jets are attributable to something other than random sampling error.

Droplet measurement accuracy, determined for the most part by negative clarity, was around 5%. This is of the same order as the standard deviation exhibited by the uniform droplet stream.

CHAPTER III

DCHX STUDIES

Background

Design of a falling droplet DCHX involves optimizing a large number of variables. These are typically classified as either operational or geometric variables[21]. Operational variables include flow rates, particle sizes, temperatures and physical properties. Geometric variables are generally limited to column length and diameter. This section outlines the governing equations for direct contact heat exchange and provides a basis for evaluating DCHX effectiveness.

Flow Rates

Combustion product flow rate is determined by fuel composition, excess combustion air and combustor size. In addition, since the DCHX configuration requires combustion products to flow upwards, sufficient draft, either natural or induced, must be present. In this study it was necessary to induce a draft using a low power fan.

The thermal capacitance ratio, C_R, defined as:

$$C_R=(\mathring{m}C_p)_L/(\mathring{m}C_p)_g \qquad (3.01)$$

is the ratio of mass flow rate times the specific heat of the liquid and gas streams. This is an important parameter

in heat exchanger operation since it is a relative measure of each stream's energy storage rate per unit of temperature change. Sekins and Thayer [10] keep this ratio constant at 1.0 for their experiments with silicon oil drops in air. A thermal capacitance ratio of 3.6 was used in Warrington and Mussulman's model of air cooling via water droplets [11]. Thermal capacitance ratio was approximately 2.0 in the present study.

Droplet Characteristics

DCHX effectiveness is a complex function of droplet size and physical properties. Terminal velocity, surface area, convective coefficient, internal mixing and conduction resistance among others are controlled by these variables.

Droplets are assumed to fall at their terminal velocity, V_T, after injection at around $V_j \doteq .75 V_T$. Terminal velocity is determined by balancing droplet gravitational and drag forces to yield:

$$V_T = [4 D_d g (\rho_d - \rho_g) / 3 C_D \rho_g]^{1/2} \qquad (3.02)$$

The drag coefficient, C_D, varies for moderate Reynold's numbers ($2 < Re_d < 500$) approximately as:

$$C_D = 18.5 / Re_d^{.6} \qquad (3.03)$$

The time period for which droplets contact the gas stream is directly related to total heat transfer. If one assumes uniform gas flow and a fixed column diameter, then contact time, t_c, is related to terminal velocity, gas velocity and column length as:

$$t_c = L/(V_T - V_g) \tag{3.04}$$

Yao [22] writes an exact formulation of the coupled droplet mass and energy transport equation. Due to the complexity of the problem however, no attempt was made at its solution. A dimensional analysis reveals the dependence of velocity, temperature and vapor concentration profiles on a number of dimensionless parameters (defined in the nomenclature):

$$Re,\ Pr,\ Sc,\ Le,\ h_{fg}(C_d - C_\infty)/\rho_d C_p (T_d - T_\infty)$$

From these parameters, $Nu = Nu(Re, Pr)$ and $Sh = Sh(Re, Sc)$, the dimensionless convective heat and mass transfer groups are found. The Lewis number, Le, is the ratio of thermal to mass diffusivity. It provides a measure of the relative thickness of the thermal and concentration boundary layers. The final parameter, $h_{fg}(C_d - C_\infty)/\rho_d C_p (T_d - T_\infty)$, is the ratio of latent to sensible energy transfer.

An approximate model of the nonsteady transport equation, assuming complete internal mixing, is derived by Yao and Schrock [23]. For the present study, the ratio $q_r/q_{tot} \ll 1$ permits omitting the radiation term. This leaves the energy equation, for a droplet, as:

$$dT_d/dt = 6/\rho_d C_p D_d [h_c (T_d - T_\infty) + h_d h_{fg} (C_s - C_\infty)] \tag{3.05}$$

For droplets in the present study, the low droplet Biot number ($Bi < .04$), evidenced by high Reynold's number ($Re_d > 10$) and low conduction resistance make this model a reasonable approximation. Coupling of mass and energy transport renders this equation difficult to solve. As a first approxi-

mation one can estimate residence time, t_R, by excluding the mass transfer term. This assumption introduces two errors which tend to cancel each other. First, it has been reported that droplet surface evaporation acts to lower heat transfer coefficients from those of nonevaporating solid spheres [24]. On the other hand energy transfer is enhanced due to latent heat addition. Since water has a relatively high heat of vaporization (h_{fg}~2400kJ/kg), a large energy input is required to cause droplets to evaporate. It is therefore reasonable to assume that drop diameter is constant in the test section [25]. Solving the energy equation under the above assumptions yields a theoretical or expected residence time as:

$$t_R=\rho_d C_p D_d/6h_c \ln[(T_{d,out}-T_\infty)/(T_{d,in}-T_\infty)] \qquad (3.06)$$

Effectiveness

The effectiveness of a heat exchanger is typically defined as the ratio of actual heat transfer rate to the maximum possible rate achieved in an infinite area exchanger, defined in terms of sensible heat recovery [26]. In this hypothetical infinite area exchanger, the hot inlet gas would be cooled to the same temperature as the cool inlet liquid. Since the liquid temperature change is of primary importance in this study, the effectiveness definition utilizes the droplet energy change in the numerator. This 'sensible' effectiveness, ε_s, is defined as:

$$\varepsilon_s=(\mathring{m}C_p)_L(T_{L,2}-T_{L,1})/(\mathring{m}C_p)_g(T_{g,1}-T_{L,1}) \qquad (3.07)$$

Since the present study was concerned with recovering latent heat from combustion products, it was necessary to define a 'latent' effectiveness, ε_L. As in the sensible case, actual heat transfer is compared to that possible from a hypothetical heat exchanger of infinite size. However in this case, the availability of the inlet gas stream is presumed to include the latent energy of the water vapor. The outlet gas stream is again assumed to leave the DCHX at $T_{L,1}$ and 100% relative humidity. Latent effectiveness, ε_L, and outlet humidity ratio , $\omega_{TL,1}$, are defined as:

$$\varepsilon_L=(\mathring{m}C_p)_L(T_{L,2}-T_{L,1})/[(\mathring{m}C_p)_g(T_{g,1}-T_{L,2})+\mathring{m}_{dg}(\omega_1-\omega_{TL,1})h_{fg,TL,1}] \quad (3.08)$$

$$\omega_{TL,1}=M_L/M_g[P_{v,TL,1}/(P_\infty-P_{v,TL,1})] \quad (3.09)$$

Effectiveness is plotted against a nondimensional heat transfer size, NTU, or number of heat transfer units. This quantity is a measure of a particular heat exchanger's actual size. A plot of ε_s versus NTU exhibits asymptotic behavior in which effectiveness is low for small NTU values, and approaches asymptotically its thermodynamic limit as NTU values become larger. For a counterflow heat exchanger, NTU values can be formulated in terms of the log mean temperature difference, ΔT_{lm}, of the two streams. Number of transfer units and log mean temperature are defined as follows:

$$NTU=(\mathring{m}C_p)_L(T_{L,2}-T_{L,1})/(\mathring{m}C_p)_g\Delta T_{lm} \quad (3.10)$$

$$\Delta T_{lm}=[(T_{g,1}-T_{L,2})-(T_{g,2}-T_{L,1})]/\ln[(T_{g,1}-T_{L,2})/(T_{g,2}-T_{L,1})] \quad (3.11)$$

Apparatus

The apparatus used for this study is part of a permanent test facility at Montana State University's Ryon Laboratory. The test apparatus consists of three major subsystems, they are the counterflow heat exchange unit, and the combustion gas and monodisperse droplet delivery systems. The entire system, which stands 4.5 meters tall, is rigidly attached to a multilevel observation platform. A detailed sketch showing platform, subsystems and instrumentation appears in Figure 9.

Counterflow Heat Exchanger

The counterflow heat exchange unit is the DCHX subsystem of greatest interest. It consists of three sections. Liquid inflow/gas outflow take place in the upper section, in the center lies the test section and the lower section provides gas inflow/liquid outflow capabilities.

A cylindrical plastic duct (36 cm i.d. x 43 cm long) to which a Rotatron 8μF capacitor fan (125 watts at operating conditions) is attached comprises the upper section. Housed inside the duct is the monodisperse droplet generating unit discussed in part I. Fan speed, for draft induction, is controlled by varying input voltage with an in line voltage regulator. A heavy duty stand, fixed to the observation platform, provides support for this assembly. Connection is made between the fan duct and test section by means

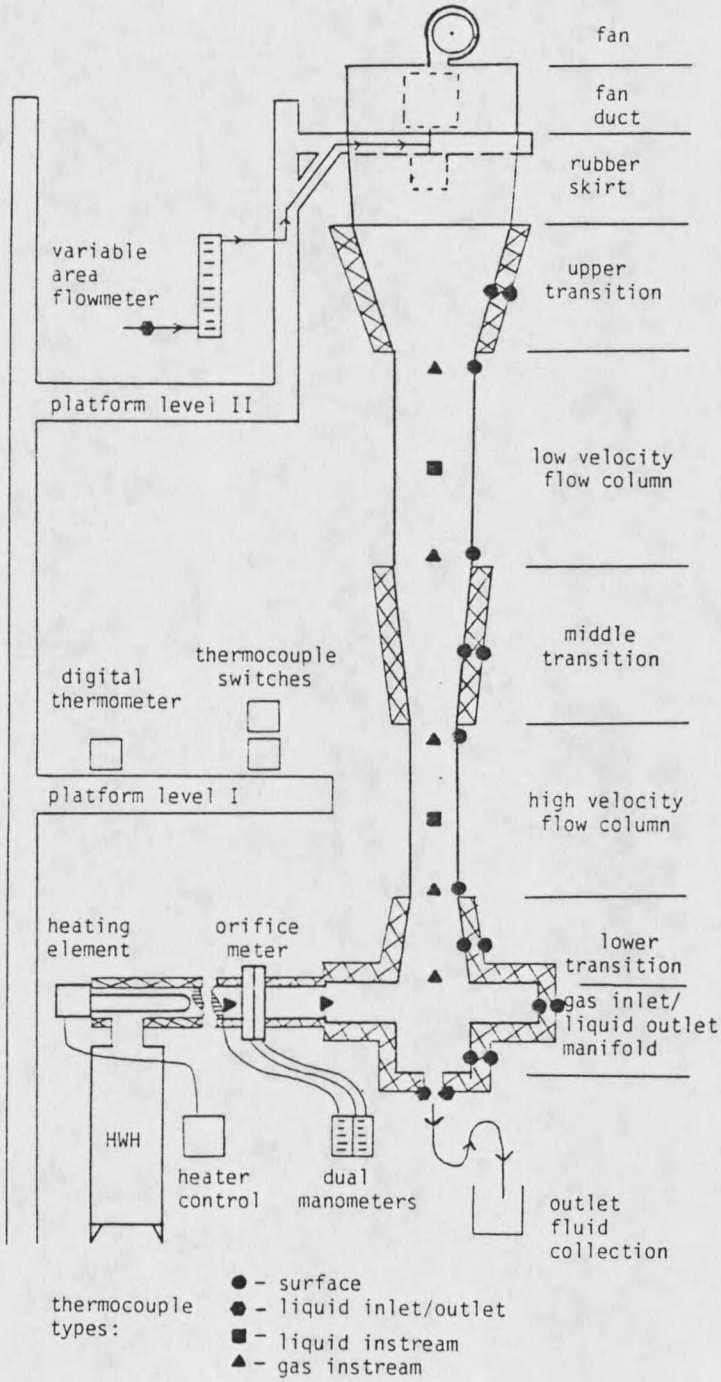

Figure 9: Direct Contact Heat Exchange Facility

of a flexible rubber skirt.

The test section is a vertical column of varying cross sectional area, consisting of three externally insulated conical sheet metal transition regions and two uninsulated transparent acrylic flow columns. Combustion gases are decelerated in the top two transition regions. Gas velocity decreases from 40 cm/s to 10 cm/s in the top region. This section is necessary to prevent water droplets, falling at about 200 cm/s, from being significantly deflected radially upon entering the test section, causing the DCHX sidewalls to become wetted. To minimize entrance effects, the gas flow is accelerated from around 20 cm/s to 180 cm/s in the bottom transition section.

Transparent acrylic was used in the flow columns to permit visual observation of droplet-gas interactions. The upper column measures 15 cm inside diameter by 96 cm long, and serves as a low velocity droplet entry region. From part I, the smallest droplet (D_d=.50 mm) has a terminal velocity of 170 cm/s. Gas velocity was kept below 50 cm/s in this column to prevent water loss by 'blowout' at the top. Average gas velocity in the lower column (7 cm i.d. x 71 cm long) was 175 cm/s. High gas velocities in this column increase contact time by holding droplets instream longer, thereby increasing total heat transfer. It is expected that a major portion of the total heat transfer occurs in this section since 80% of its contact time is spent in the high velocity column and two adjacent transition regions.

A specially designed manifold permits combustion gas entrance to, and working fluid exit from, the DCHX test section. The cylindrical manifold, welded from 6.4 mm steel plate, has a mass of 35 kg and consists of a double wall upper and single wall lower chamber. Combustion gas enters through the upper chamber's insulated outer wall into a .021 m^3 annular region. Perforations in the chamber's inner wall allow a uniformly distributed stream of gas into the test section. Water droplets bypass the upper chamber through its inner section, and are collected in the lower chamber. Fluid temperature is measured at the manifold outlet by two thermocouples immersed in such a way that continuous liquid flow is allowed past them. Outlet fluid is collected for the entire test run to accurately determine its average flow rate. A water trap prevents gas from escaping through the liquid outlet.

Test section gas and surface temperatures were monitored throughout each test run. Great care was exercised in thermocouple placement and assembly to minimize errors associated with conduction loss, contact resistance and fabrication inconsistencies. All thermocouples were type T, welded in an Argon environment and checked in a constant temperature bath. Thermocouple placement, in all cases, was made such that a section of uninsulated lead wire (minimum length of 20 wire diameters) was exposed to the same conditions as the bead junction. This arrangement provided an isothermal region adjacent to the junction whose purpose

was to eliminate conduction losses.

All insulating surfaces (transition regions and manifold) had thermocouples located on their inner and outer surfaces. Steady state heat loss through these surfaces was evaluated from these temperatures and thermal resistance information. Flow column temperature measurement occurred at the column inner and outer surface and gas stream centerline. Good thermal contact was achieved for surface measurements by machining a small groove in the acrylic surface, perpendicular to the gas flow direction. Bead junction and bare lead wire were then epoxied into this groove. Surface temperature accuracy was checked in a series of tests using a single platinum, foil type, resistance temperature detector.

Gas stream temperatures were monitored with thermocouple probes configured to prevent bead junctions from contacting droplets (Figure 10). Thermocouples were epoxied to and insulated from lengths of 3.2 mm stainless steel tube. To allow a sufficient length of lead wire exposed to the gas stream, thermocouple bead junctions were located 9.5 mm from the tube's end. After bending the tube to a right angle, a teflon sleeve (7 mm i.d. x 4 mm o.d. x 19 mm long) was fitted such that a water tight seal was formed.

An attempt was made to determine droplet temperatures at one axial location for each acrylic column. A sketch of this probe design, construction of which is similar to that of the gas probes, is shown in Figure 10. The droplet probe

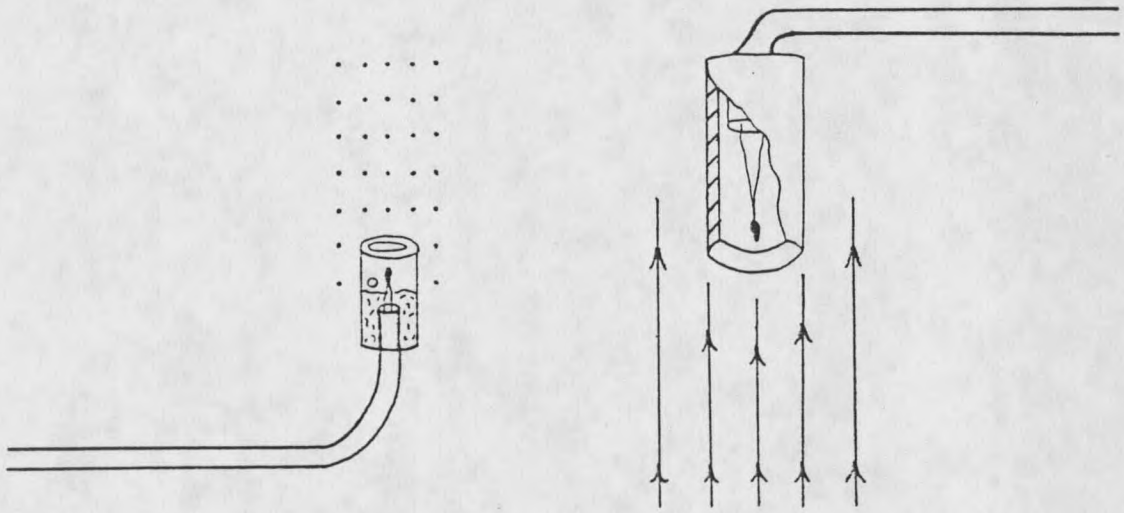

Figure 10: Liquid and Gas Temperature Thermocouple Probes

was constructed by fitting a small plastic sleeve over a 2.5 mm tube, also bent to a right angle. In this case the probe is turned upwards to catch droplets. The plastic sleeve has a 1.3 mm hole along its side to allow continuous flow through. The sleeve reservoir has a capacity of around 40 droplets.

Gas and Fluid Delivery

A 40,000 BTU/hr domestic hot water heater (HWH) supplies natural gas combustion products to the DCHX test section. Insulated steel pipe, 7.9 cm i.d. by 4.5 meters long, connects the HWH exit port to the DCHX manifold. In some cases it was necessary to run atmospheric air through the test section. Since the HWH combustion chamber is open to the atmosphere, shutting down the combustor permitted air to be drawn by the suction fan. A temperature limited, thermostatically controlled, Chromalox 6kW immersion heater at the HWH exit maintained DCHX inlet temperature at the desired level. Gas flow rate measurements were made with a flange tap orifice flowmeter (ΔP=2.5 cm-H_2O at .55 m^3/min). Orifice differential and inlet pressure were measured with a pair of U-tube water manometers. Gas temperature upstream of the flowmeter and at the DCHX inlet were each found with single thermocouple probes. Unlike other gas stream probes these had no right angle bends or bead shields. Readings from these probes agree to within 1%(°K) of those with a mercury bulb thermometer. A radial probe traverse revealed

only a minimal temperature gradient at these locations.

Fluid delivery is accomplished by means of the droplet injector housed in the upper fan duct. Injector flow rate is monitored with a Tri-Flat variable area flow meter. Flowmeter calibration tests show injector flow rate to be independent of vibration frequency. A single thermocouple measures water temperature at the DCHX inlet. For heat exchange studies, 31 injectors were used to provide adequate water flow to the test section.

Specially constructed digital psychrometers measured wet and dry bulb temperatures at the DCHX inlet and outlet. For these psychrometers, thermocouple bead junctions were lead soldered inside a .95 cm length of copper rod (surface area =1.8 cm^2). A sock type wick, secured to the rod, served as the wet bulb. The outlet psychrometer, located in the upper transition section, used a 4.5 volt DC fan to provide convective transport. The inlet psychrometer is a separate unit, through which a suction pump draws gas samples for measurement. Using data on natural gas fuel composition and flow rate and combustion product flow rate, a stoichiometric equation balance provided a means of verifying the psychrometric determination of combustion product vapor content.

Finally, a pair of Omega 24 position switches connected all thermocouples to a Fluke model 2168A digital thermometer for temperature determination.

Experimental Procedure

Historically, characterizing two phase flows has been considered an 'insecure science'. Accurate measurement of individual phase properties, in a multi-phase system, is subject to considerable uncertainty [27]. Before engaging in a full fledged DCHX study, it seemed prudent to first conduct single phase tests, for the purpose of assessing instrumentation performance. To this end, tests were carried out with the DCHX using a gaseous phase only (air). Inlet gas temperatures were varied slightly about the data center case. Subsequent energy balance information provided insight concerning gas flow and temperature measurement.

At this point the monodisperse droplet generator was coupled with the DCHX and a series of two phase tests conducted. Parameter variations for these studies were extensive, the most significant being droplet size dispersion. Another important variation involved using heated air in place of combustion products to find the effect of gas humidity on effectiveness. Other tests were designed to determine the system's sensitivity to changes in inlet gas temperature, and inlet liquid flow rate.

In carrying out these investigations great care was taken to allow sufficient time for the apparatus to reach steady state conditions. This is true for both initial start up and for parameter variations after reaching initial equilibrium. Conservative estimates of system time con-

stants for these changes are five hours for start up and thirty minutes for variations. Typical equilibrium times during test runs were eight hours and one hour respectively. Start up time constant is significantly higher since it includes heating the entire gas delivery system in addition to the DCHX. Parameter changes involve much smaller temperature changes and a much smaller thermal mass. This is so because once the gas delivery system is brought to temperature it does not change throughout the remaining test runs.

Test duration was twenty minutes in both studies. Due to a high thermal mass, fluctuations in system properties was minimal once equilibrium was reached. Therefore manual data acquisition, at five minute intervals, was deemed adequate. Since tests for this experiment occurred over a period of several months, it was necessary to have a control case to account for atmospheric property change effects. To accomplish this, the DCHX was brought to equilibrium at a prescribed set of initial conditions first. Data collected at these conditions provided the necessary control.

Data were reduced using the computer code BALANCE, written by the author. BALANCE receives DCHX temperature, humidity, pressure and flow rate data as input. Output consists of gas and vapor flow rates, single phase heat loss and a test section energy and mass balance. A copy of the code, including documentation appears in the appendix.

Results and Discussion

Results of the direct contact heat exchange studies are divided into two parts. Preliminary results are single phase energy and two phase mass balances. These results are included to show that temperature, gas and liquid flow instrumentation operated within acceptable limits.

The purpose of the primary DCHX study was to determine the heat exchanger's effectiveness, with respect to latent heat recovery, under various operating conditions. Of particular interest were the effect of droplet size uniformity and inlet gas humidity on performance. Results are presented in terms of the sensible and latent effectiveness defined earlier, as a function of number of transfer units (NTU). Comparison is made between the present system and a conventional counterflow unit described by Kays and London [26].

Energy and Mass Balances

Single phase energy balance results are presented in Table 2 as percent deviation between predicted and measured DCHX heat loss, defined as follows:

$$q_p=(T_s-T_\infty)/(R_w+R_e) \tag{3.12}$$

where: $R_e=R_rR_{nc}/(R_r+R_{nc})$

$$q_m=(\mathring{m}C_p)_g(T_{g,out}-T_{g,in}) \tag{3.13}$$

Due to uncertainties in calculating thermal resistances and the determination of meaningful radiation emissivities

for the acrylic sections, the energy balances within about 6% in Table 2 are within the limits of acceptability.

Table 2: Single Phase Energy Balance of Predicted vs. Measured DCHX Heat Loss

$T_{g,in}$ (°K)	Predicted Loss (W)	Measured Loss (W)	Percent Deviation (%)
386	123	125	1.6
394	130	133	2.3
401	136	145	6.2

Table 3 lists mass balance data for 22 combustion product and four air two phase test runs. The table shows typical mass balance results on an absolute and percent basis. The effect of inlet liquid flow rate on the DCHX condensation/evaporation process is also shown. Mass balance on a percent basis falls within 6%. Confidence intervals for liquid flow rates are within 2% and inlet vapor flow rate 4% from the given values. The majority of the mass balance discrepancy can be attributed to outlet vapor flow measurement error. Error was incurred through flow nonuniformities and possible gas dilution. Flow nonuniformities at the DCHX outlet would have caused humidity ratio to vary with location, making the indicated readings different from the true average reading. Also, even though the DCHX test section was tested and found to be airtight, some dilution by outside air could have occurred, thereby lowering the outlet gas humidity ratio. The last column in Table 3 gives the amount of water condensed as a percent of

inlet liquid flow rate. A positive quantity in this column indicates a net increase in liquid water for the test run. Column one is arranged, in terms of inlet liquid flow rate, from lowest to highest. Thus the tendency shown by the liquid gain column in going from negative at the top to positive toward the bottom indicates higher condensation rates for higher inlet liquid flow rates.

Table 3: Two Phase DCHX Mass Balance Data

Mass Liquid in (gm/s)	Mass Liquid out (gm/s)	Mass Vapor in (gm/s)	Mass Vapor out (gm/s)	Mass Water Not Balanced (gm/s)	Percent Mass Balance (%)	Percent Liquid Gained (%)
Combustion Product Values						
2.45	2.44	.316	.264	.062	2.3	-0.41
2.50	2.45	.317	.277	.090	3.3	-2.00
2.63	2.60	.328	.198	.160	5.6	-1.14
2.63	2.56	.325	.217	.178	6.2	-2.66
2.68	2.63	.315	.229	.136	4.6	-1.87
2.70	2.66	.324	.233	.131	4.4	-1.48
2.72	2.67	.323	.248	.125	4.2	-1.84
2.76	2.71	.318	.249	.119	4.0	-1.81
2.76	2.70	.321	.298	.083	2.7	-2.17
2.79	2.74	.314	.302	.061	2.0	-1.79
2.99	3.06	.330	.170	.089	2.7	2.34
2.99	3.02	.329	.185	.114	3.5	1.00
3.01	3.04	.312	.179	.103	3.1	1.00
3.01	3.04	.327	.230	.068	2.0	1.00
3.01	3.02	.325	.226	.089	2.7	0.33
3.03	3.04	.332	.189	.133	4.0	0.33
3.03	3.06	.321	.166	.125	3.8	1.00
3.10	3.08	.315	.235	.100	3.0	-0.65
3.19	3.18	.319	.224	.105	3.0	-0.31
3.19	3.21	.323	.150	.153	4.5	0.63
3.19	3.23	.323	.173	.110	3.2	1.25
3.21	3.24	.314	.232	.051	1.5	0.93
Air Values						
2.97	2.85	.031	.100	.051	1.7	-4.04
2.99	2.87	.031	.128	.022	0.7	-4.01
2.99	2.88	.031	.093	.048	1.6	-3.68
3.01	2.91	.031	.118	.013	0.4	-3.32

Primary Studies

The variation of sensible and latent effectiveness for combustion products and air with both uniform and non-uniform droplets is shown in Figures 11 and 12. Several observations concerning DCHX effectiveness are immediately clear.

A linear regression analysis on uniform and nonuniform droplet data from Figure 11 shows a difference of less than 1% in effectiveness between the two modes of operation. Several possible causes for this lack of effect are apparent. First it may be that, for existing flow conditions, the difference in size dispersion between uniform and non-uniform droplets is not large enough to significantly influence DCHX effectiveness. In other words, an increase of droplet size dispersion from around 5% to the 10 to 20% shown in Chapter II, was not sufficient to cause a measurable change in effectiveness. On the other hand, nonuniform droplet diameters exhibit a skewed distribution in which droplets smaller than the mean are most often produced. It is possible then, that the loss in effectiveness of a few large drops is offset by the increase realized by the large number of small drops produced by the nonvibrating jets. A third possible cause involves assumptions made in designing the DCHX test section. Gas flow was assumed to be axially symmetric with negligible radial velocity gradients. Consequently, even if droplet size dispersion was theoretically

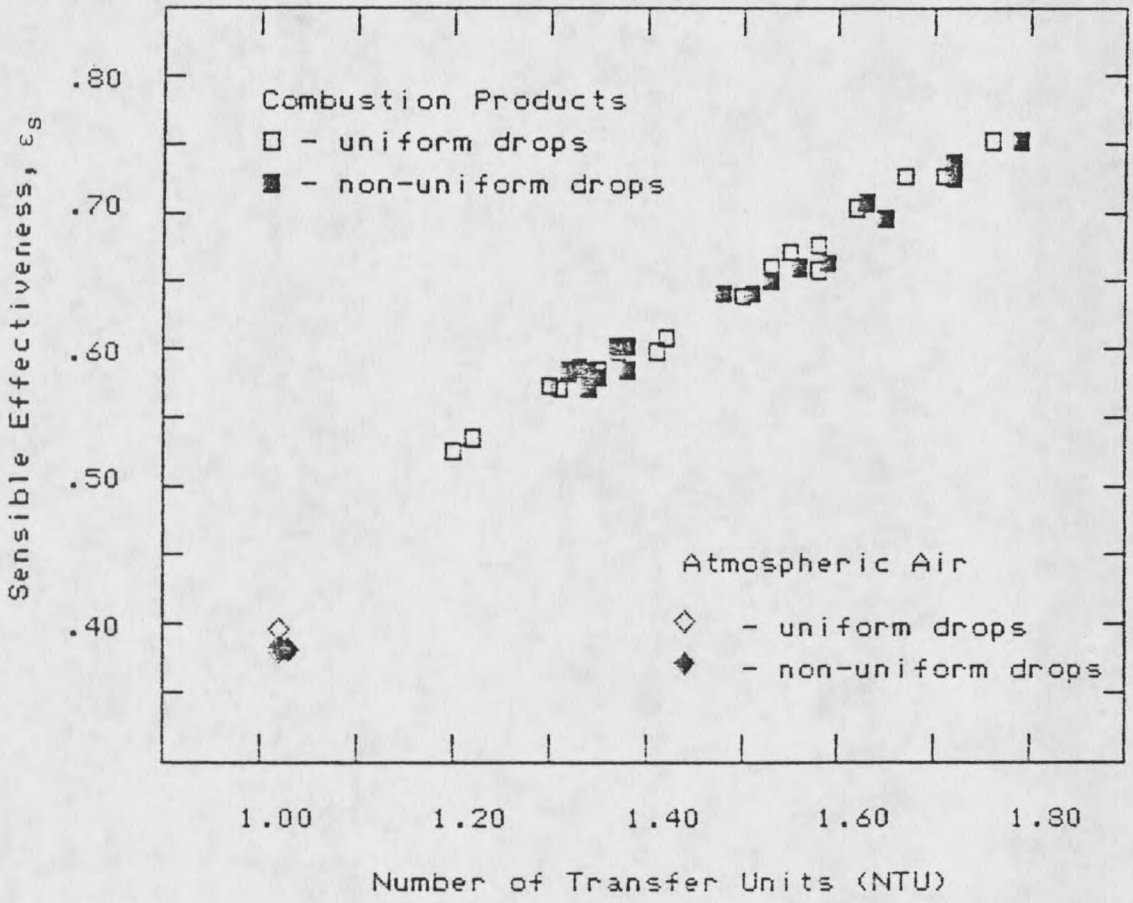

Figure 11: DCHX Sensible Effectiveness vs. Number of Transfer Units

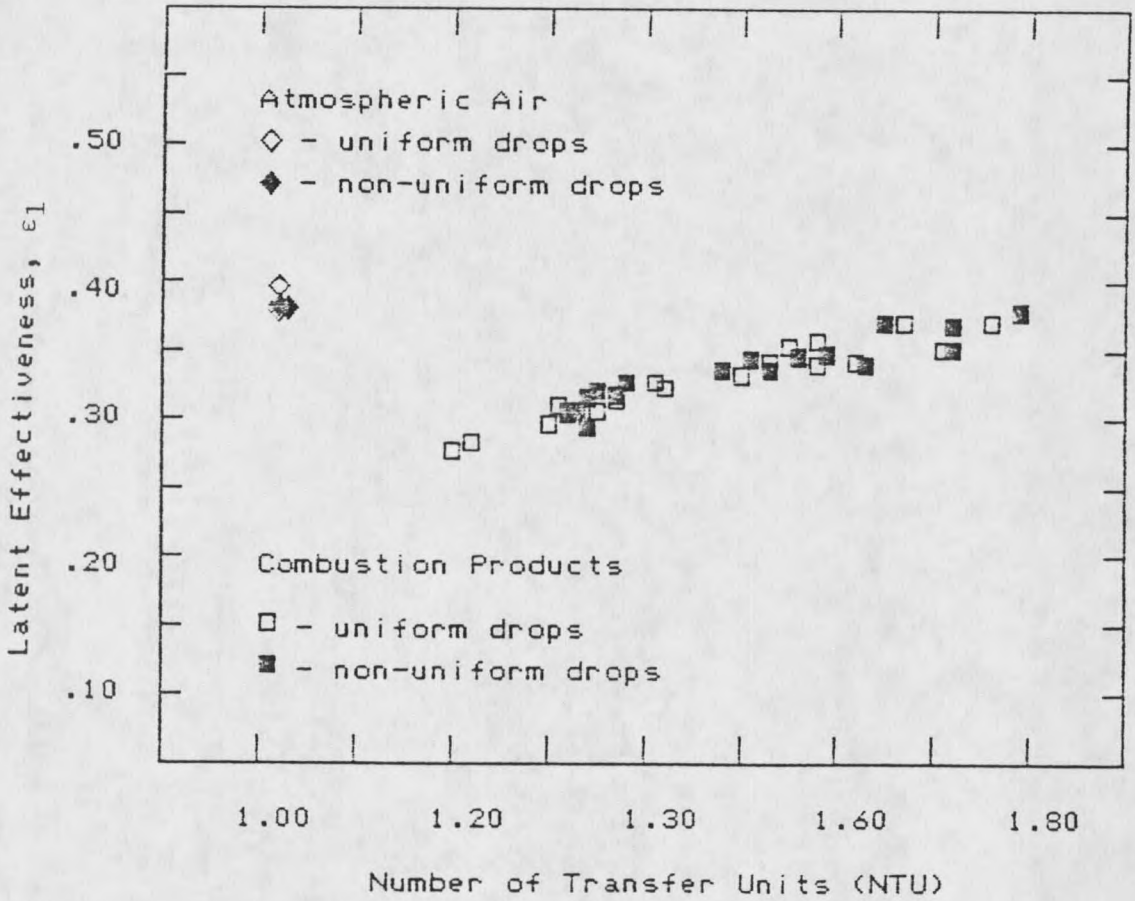

Figure 12: DCHX Latent Effectiveness vs. Number of Transfer Units

large enough to influence DCHX performance, radial and axial variations in flow conditions may have negated the droplet dispersion effects. In this case the implication is that the DCHX was operating at less than optimum conditions. Finally, in all modes of operation a portion of the liquid flow unavoidably contacted and flowed down the test section inner wall. This phenomenon may have appreciably reduced the surface area available for heat transfer in both the uniform and nonuniform droplet cases, thus minimizing the difference between the two.

It is clear from the figures that the effectivenesses for combustion products differ considerably from those of air. However the reasons why, as shown in Figures 11 and 12, ε_s is higher than ε_L for combustion products while $\varepsilon_s \sim \varepsilon_L$ for air may not be clear. This apparent discrepancy in effectiveness values for combustion products can be explained by first noting that the inlet air humidity ratios are an order of magnitude lower than those for combustion products (Table 3). As the high temperature air enters the test section ($T_{g1} \sim 395°K$), its saturation pressure is large, and a considerable amount of sensible energy from the air stream is lost to the evaporation of water in order to bring the air's vapor pressure up close to its saturation pressure. Combustion products on the other hand, have a higher initial vapor content than that found in a saturated stream at the outlet gas temperature. This results in a net condensation of vapor from combustion products. The energy

gained in condensing rather than evaporating water is available to raise droplet temperatures. Sensible effectiveness is consequently much higher for combustion products since the droplet temperature change is higher.

As for the latent effectiveness, since the inlet vapor content for air is so low, air has little potential from which to recover latent energy. Therefore the difference between ε_L and ε_s for air is negligible. Combustion products, however contain a significantly higher amount of energy in the latent form. The low values of ε_L for combustion products, in comparison to air, indicate that the DCHX is doing a relatively poor job of recovering latent energy. Even though temperatures and flow rates of the outlet liquid are higher for combustion products, there is potential to increase effectiveness by recovering more latent energy.

A comparison of DCHX sensible effectiveness results with those from an ideal counterflow unit, in the same NTU range and having an equivalent thermal capacitance ratio, described by Kays and London [26] appears in Figure 13. It should first be noted that the ideal curve assumes no losses in the heat exchanger. Since the present system does experience irrecoverable losses, which are not corrected for, it is expected that effectiveness values would fall below those of the ideal.

In addition, with regard to the determination of log mean temperature difference, the temperature measurement having the greatest uncertainty was that of the outlet gas,

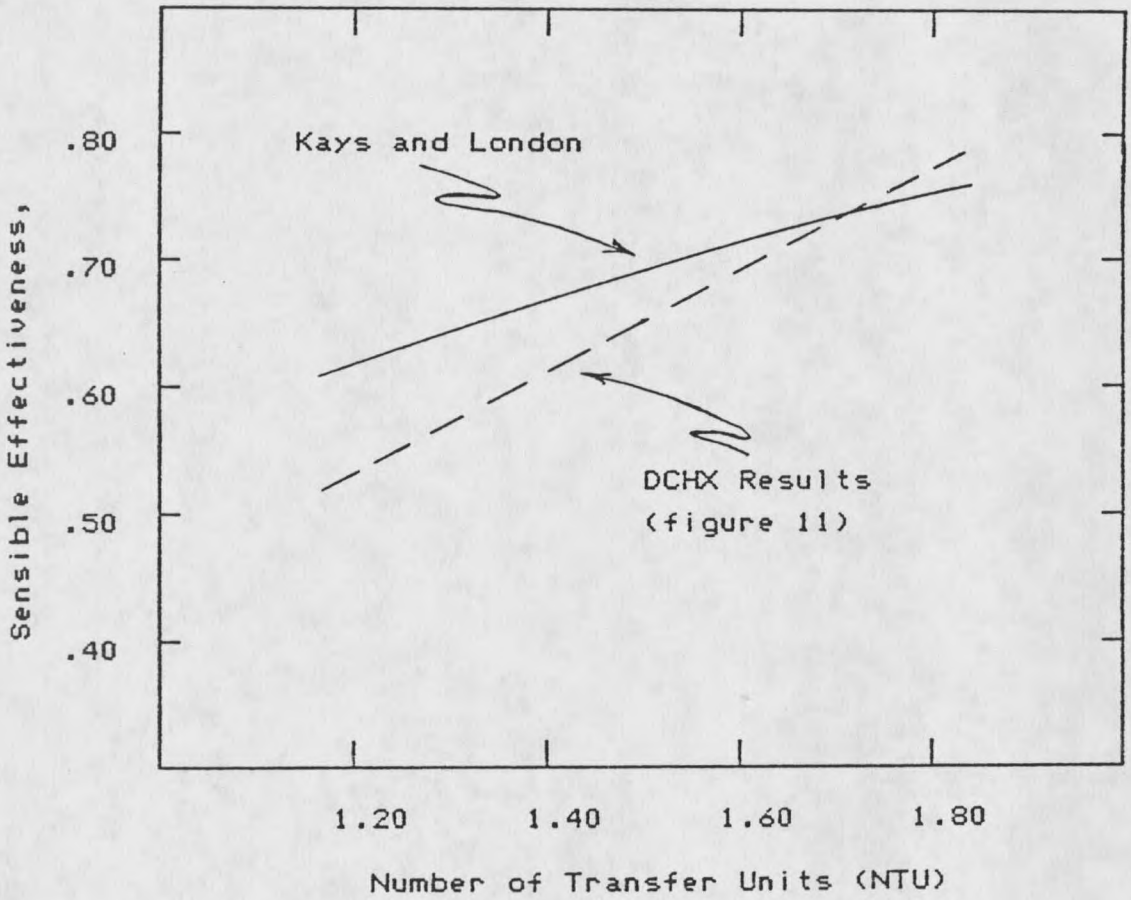

Figure 13: Theoretical and Experimental Sensible Effectiveness for a Counterflow Heat Exchanger

$T_{g,2}$. Due to axial and radial variations in outlet gas temperature, and the general difficulty in obtaining reliable temperature measurements in two phase flows, the value of $T_{g,2}$ was taken as the test section outlet's inner surface temperature. This surface temperature was less than the outlet gas temperature by an amount on the order of 3%(°K) of the net DCHX gas temperature change. This results in an overprediction of NTU values of around 10%(°K). This influences the DCHX effectiveness curve in Figure 13 by shifting it toward the right. In other words, effectiveness may be underpredicted, for given NTU values, by the curve shown.

The important observation to be made in Figure 13 is that, for the range of NTU shown, the DCHX curve is essentially linear with a steeper slope than the Kays and London curve. Since ε vs. NTU plots exhibit asymptotic behavior, it is apparent that the DCHX is further from its thermodynamic limit than the ideal heat exchanger.

Finally Figures 14 and 15 show the effect of inlet liquid flow rate and gas temperature on sensible effectiveness. With all other parameters constant, an increase in liquid flow rate increases effectiveness. This is because higher liquid flow raises the energy storage capacity of the system which makes it possible to extract more energy from the hot gas. In addition since the outlet gas contains less energy, its temperature is lower and latent energy recovery is enhanced. Figure 15 demonstrates that an increase in inlet gas temperature, even though providing a greater

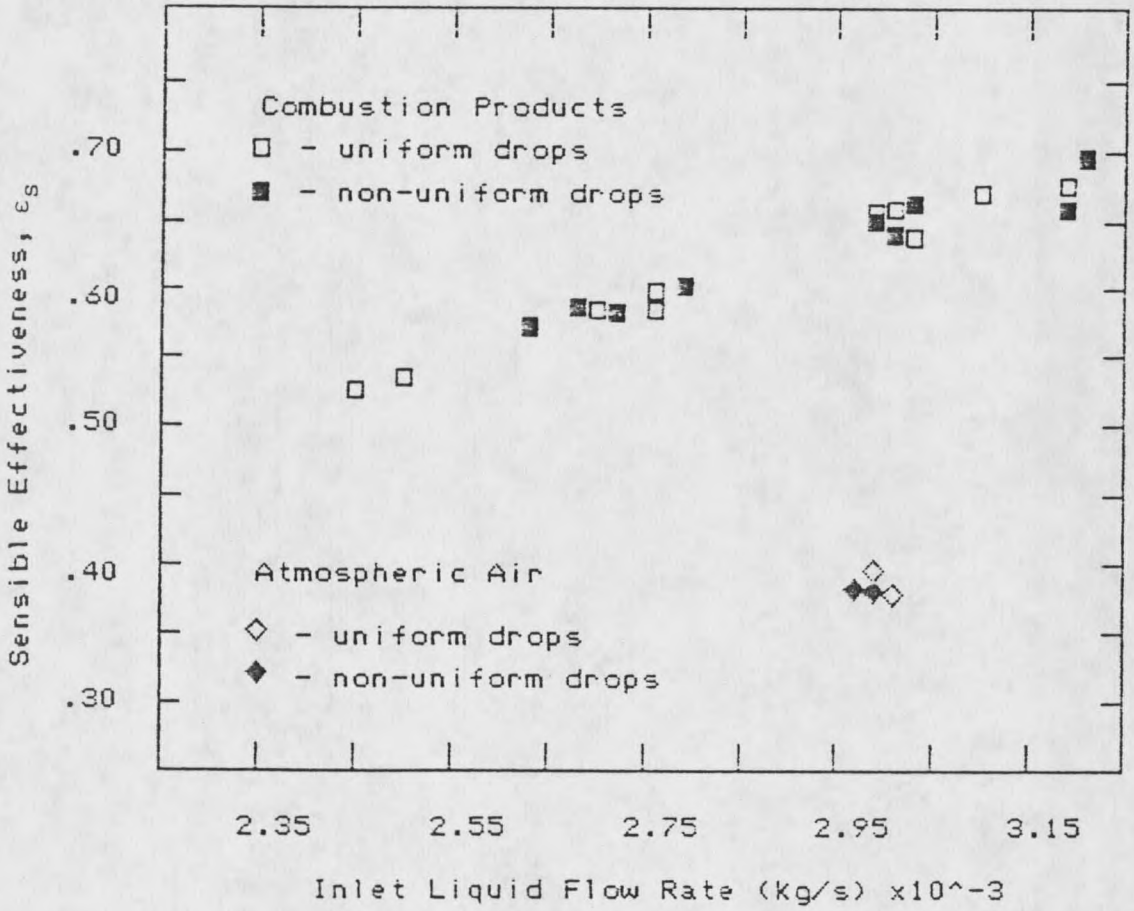

Figure 14: DCHX Sensible Effectiveness vs. Inlet Liquid Flow Rate

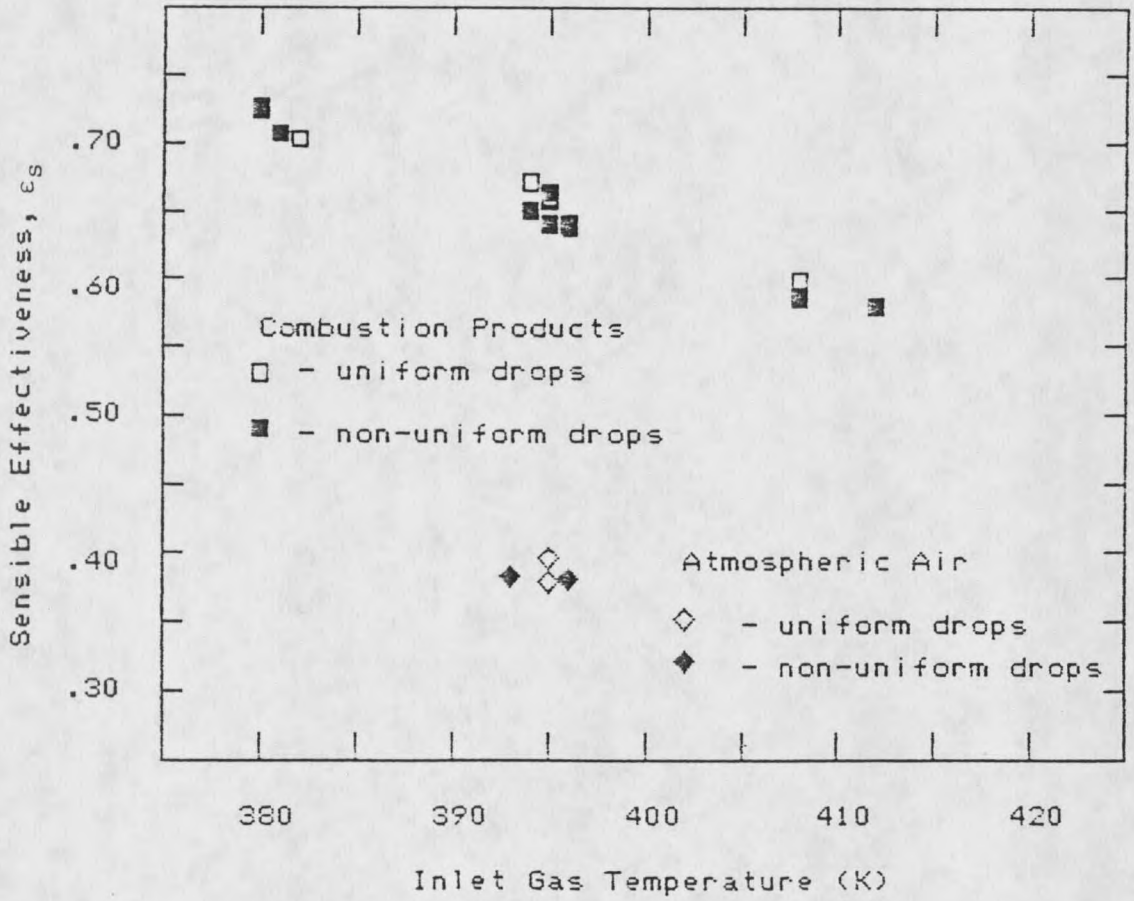

Figure 15: DCHX Sensible Effectiveness vs. Inlet Gas Temperature

amount of sensible energy, causes a decrease in effectiveness. Thus, for fixed gas and liquid flow rates, increased inlet gas temperature causes a corresponding increase in outlet temperature, and subsequent decrease in latent energy recovery.

CHAPTER IV

CONCLUSION

The present investigation has provided data regarding uniform droplet production and the influence of certain operational variables on DCHX performance.

In the first part of this study a droplet generator was tested to determine its droplet production characteristics for various jet velocities, vibration frequencies and power inputs. Results show that uniform droplets, with standard deviations around 5%, are produced when the droplet generator is axially vibrated. Variations in jet velocity of 15%, vibration frequency of 20% and power input of 40% had no effect on droplet monodispersity. In addition, drop diameter is shown to be weakly dependent on jet velocity and vibration frequency but independent of input power. It is therefore reasonable to conclude that droplet uniformity is insensitive to small changes in the above parameters.

It has also been shown that a stream of nonuniform droplets is produced when water is forced through the generator without being vibrated. The nonuniform drops exhibit a skewed distribution and standard deviations that vary from around 10 to 20% of their mean value. The size dispersion of nonuniform drops appears to be somewhat dependent on jet velocity.

The second part of this investigation consisted of a number of DCHX performance tests in which droplet uniformity and inlet gas vapor content along with inlet liquid flow rate and gas temperature were varied. Results indicate that heat exchanger effectiveness is not dependent on droplet uniformity for the range of size dispersions attained. However it is possible that, due to flow nonuniformities, droplet size was not optimized for the actual flow conditions. Consequently effectiveness results were less sensitive to uniformity effects than they might otherwise have been. Other results show, as could be expected, effectiveness is a strong function of inlet gas vapor content.

Sensible effectiveness for combustion products is approximately twice that attained for air at otherwise identical conditions. DCHX effectiveness evaluated in terms of latent heat recovery shows combustion product results below those for air. The present system therefore, has the potential to attain significantly higher effectivenesses by recovering a greater portion of the available latent energy. Tendencies in the data indicate that increasing inlet liquid flow rate is one way to increase latent energy recovery in the present system. Another means of increasing DCHX effectiveness would be to increase the test section length. This is suggested by the decrease in effectiveness shown at higher inlet gas temperatures.

Overall, the present system shows excellent recovery of available energy despite indications the system was operated

at less than optimum conditions. It seems apparent that still better recovery could be accomplished by increasing droplet flow rate and contact time.

REFERENCES

REFERENCES

1. L.M. Hossffeld and D.J. Hawkins, 'A Cost Effective Technology for Flue Gas Recovery', ASME, 85-JPGC-Fu-1, 1985.

2. R.J. Goldstick and A. Thuman, The Waste Heat Recovery Handbook, Fairmont Press, Atlanta, 1983)pg. 87.

3. G. Brown, 'Heat Transmission by Condensation of Steam on a Spray of Water Drops', in General Discussion on Heat Transfer, Institute of Mechanical Engineering, London, 1951, pp. 49-53.

4. S. Calvert, 'Particle Control in Scrubbing', in Handbook of Pollution Control Technology, S. Calvert and H.M. Englund, eds.(John Wiley, New York, 1984)pg. 219.

5. B.B. Crocker and K.B. Schnelle, 'Control of Gases by Absorbtion, Adsorbtion and Condensation', in Handbook of Pollution Control Technology, S. Calvert and H.M. Englund, eds. (John Wiley, New York, 1984)pp. 159-160.

6. J.R. Fair, 'Designing Direct Contact Coolers/Condensers', Chemical Engineering, vol. 2, June 1972, pp. 91-100.

7. S. Sideman and D. Moalem-Maron, 'Direct Contact Condensation', in Advances in Heat Transfer, J.P. Hartnett and T.F. Irvine, eds.(Academic Press, New York, 1982)pp. 235-236.

8. S.L. Goren and G.R. Wilke, 'Sea Water Evaporation by Immiscible Liquid Heat Transfer', in Sea Water Conversion Laboratory Report No.67-1, Water Resource Center, University of California at Berkeley, Desalination Report No.14(1967), pp. 31-33.

9. K.M. Sekins and W.J. Thayer, 'Heat Transfer Rates in a Droplet Heat Exchanger', ASME, 85-HT-48, 1985.

10. W.J. Thayer,K.M. Sekins and A.P. Bruckner, πDevelopement of High Effectiveness Droplet Heat Exchangersπ, Final Report submitted to DOE(contract No.DE-AC06-81ER10918), January 1985, pp. 3-12 to 3-17.

11. R.O. Warrington and R.L. Mussulman, 'Analysis of a Liquid/Gas Direct Contact Heat Exchanger Concept', Journal of Energy, vol. 7, Nov.-Dec.1983, pp. 732-734.

12. Lord Rayleigh, 'On the Instability of Jets', Proceedings of the London Math Society, vol. 10, No.4(1878), pp. 4-13.

13. R. Rajagopalan and C. Tien, 'Production of Monodispersed Drops by Forced Vibration of a Liquid Jet', Canadien Journal of Chemical Engineering, vol. 51, June 1973, pp. 272-279.

14. J.M. Schneider and C.D. Hendricks, 'Source of Uniform Sized Liquid Droplets', Review of Scientific Instruments, vol. 35, October 1964, pp. 1349-1350.

15. N.R. Linblad and J.M. Schneider, 'Production of Uniform Sized Liquid Droplets', Journal of Scientific Instruments, vol. 42, pp. 635-638.

16. E.K. Dabora, 'Production of Monodisperse Sprays', The Review of Scientific Instruments, vol. 38, April 1967, pp. 502-506.

17. L. Strom, 'The Generation of Monodisperse Aerosols by Means of a Disintegrated Jet of Liquid', The Review of Scientific Instruments, vol. 40, June 1969, pp. 778-782.

18. D.B. Harmon, 'Drop Sizes from Low Speed Jets', Journal of the Franklin Institute, vol. 259, 1955, pp. 519-522.

19. S.L. Goren and S. Wronski, 'The Shape of Low Speed Capillary Jets of Newtonian Liquids', Journal of Fluid Mechanics, vol. 25, 1966, pp. 185-198.

20. V.G. Levich, Physicochemical Hydrodynamics, (Prentice-Hall, Englewood Cliffs, N.J., 1962) pg. 633.

21. R. Letan, 'Design of a Particulate Direct Contact Heat Exchanger: Uniform Countercurrent Flow', ASME, 76-Ht-27, 1976.

22. S.C. Yao, Ph.D. Thesis, University of California at Berkeley, 1974.

23. S.C. Yao and V.E. Schrock, 'Heat and Mass Transfer from Freely Falling Drops', ASME, 75-WA/HT-37, 1975.

24. M.C. Yuen and L.W. Chen, 'Heat Transfer Measurements of Evaporating Droplets', International Journal of Heat and Mass Transfer, vol. 21, 1978, pp. 537-542.

25. S.C. Yao and A. Rane, 'Heat Transfer of Evaporating Droplet Flow in Low Pressure Systems', ASME, 79-WA/HT-10, 1979.

26. W.M. Kays and A.L. London, Compact Heat Exchangers, (McGraw-Hill, New York, 1955)pp. 13-63.

27. G.B. Wallis, 'Review-Theoretical Models of Gas-Liquid Flows', Journal of Fluids Engineering, vol. 104, Sept. 1982, pp. 279-283.

APPENDICES

APPENDIX A

DROPLET DATA

Uniform Droplet Data

	D_{mean} (mm)	σ (%)	D_{max} (mm)	D_{min} (mm)	Sample Size
Frequency (Hz)					
680	.650	5.9	.742	.589	32
765	.622	5.0	.696	.556	54
850	.607	4.7	.676	.523	47
935	.597	4.3	.655	.523	54
1020	.577	3.3	.615	.518	51
Input Power (W)					
0.9	.605	4.3	.688	.543	45
1.1	.615	3.8	.665	.572	47
1.5	.610	3.7	.671	.566	54
1.9	.605	3.9	.650	.559	54
2.2	.605	4.3	.688	.554	50
Jet Velocity (m/s)					
1.79	.648	5.5	.721	.572	36
1.65	.638	5.1	.711	.566	33
1.52	.622	5.5	.691	.541	36
1.38	.607	4.8	.665	.551	36

Non-Uniform Droplet Data

Jet Velocity (m/s)	D_{mean} (mm)	D_{mode} (mm)	σ (%)	D_{max} (mm)	D_{min} (mm)	Sample Size (-)
1.77	.486	.468	13	.635	.401	48
1.63	.490	.451	11	.635	.434	50
1.47	.527	.451	20	.802	.418	48
1.31	.559	.485	17	.819	.434	40

APPENDIX B

EFFECTIVENESS DATA

$T_{g,1}$ (°F)	$T_{g,2}$ (°F)	$T_{L,1}$ (°F)	$T_{L,2}$ (°F)	$\dot{m}_{g,1}$ x10³ (kg/s)	$\dot{m}_{L,1}$ x10³ (kg/s)	$\dot{m}_{L,2}$ x10³ (kg/s)	$\dot{m}_{v,1}$ x10³ (kg/s)	$\dot{m}_{v,2}$ x10³ (kg/s)	uni-form-ity
Combustion Product Values									
251	102	51	119	5.98	2.63	2.60	.328	.198	nu
251	106	49	119	6.03	2.63	2.56	.325	.217	u
248	102	50	117	6.05	2.76	2.70	.321	.298	u
249	105	51	118	6.02	2.79	2.74	.314	.302	nu
245	102	49	117	5.92	3.19	3.18	.319	.224	u
249	104	51	117	6.06	2.45	2.44	.316	.264	u
246	104	49	117	6.04	2.68	2.68	.315	.229	nu
247	104	50	118	6.10	2.76	2.71	.318	.249	u
250	104	50	118	6.09	2.50	2.45	.317	.277	u
249	102	50	117	6.04	3.10	3.08	.315	.235	u
251	106	50	118	6.01	2.70	2.66	.324	.233	u
253	105	49	119	6.09	2.72	2.67	.323	.248	nu
253	101	52	118	6.10	3.01	3.04	.312	.179	nu
254	102	52	118	6.06	3.03	3.04	.332	.189	u
251	100	52	116	6.10	3.19	3.21	.323	.150	nu
252	102	52	118	6.09	3.19	3.23	.323	.173	u
251	100	52	119	6.05	3.03	3.06	.321	.166	nu
252	100	53	119	6.01	2.99	3.06	.330	.171	u
252	102	52	122	5.44	2.99	3.03	.313	.128	nu
251	104	53	121	5.43	2.99	3.07	.322	.164	u
253	105	52	119	6.58	3.03	3.03	.331	.244	nu
252	103	52	120	6.55	3.01	3.02	.341	.224	u
226	100	51	115	6.19	3.01	3.06	.339	.181	nu
228	101	51	116	6.15	2.99	3.01	.332	.169	u
253	103	49	118	6.71	2.97	2.95	.338	.229	nu
253	103	49	117	6.73	2.97	2.95	.339	.249	u
225	97	51	115	6.14	3.01	3.09	.331	.163	nu
225	98	51	116	6.08	2.97	3.02	.328	.178	u
250	101	51	118	6.10	2.99	3.02	.329	.185	nu
251	103	51	119	6.07	3.01	3.04	.327	.230	u
274	104	51	121	6.08	2.99	2.97	.322	.219	nu
274	104	51	121	5.90	2.97	2.99	.329	.223	u
252	100	50	118	6.12	3.21	3.24	.314	.232	nu
252	103	51	118	6.13	3.01	3.02	.325	.226	nu
252	103	51	120	5.49	2.99	3.04	.316	.181	nu
282	107	52	122	6.04	3.05	3.04	.337	.228	nu
Air Values									
253	80	54	94	6.26	2.99	2.88	.031	.093	nu
252	81	55	94	6.26	3.01	2.91	.031	.118	u
248	80	53	93	6.28	2.97	2.85	.031	.100	nu
251	82	52	93	6.14	2.99	2.87	.031	.128	u

APPENDIX C

BALANCE DATA REDUCTION CODE

```
10 '  BALANCE.......DCHX Data Reduction Program
20 '
30 '  This program receives DCHX temperature, humidity,
      pressure
40 '  and flow rate data as input
50 '  BALANCE can be used to perform single or two phase
      analyses
60 '  Output options include:
70 '        1. mass flow, energy and mass balances
80 '           and effectiveness results only
90 '        2.DCHX thermal resistences and heat transfer
               plus #1
100'        3. DCHX gas properties and non dimensional
               parameters plus #1,2
110 '
120 '
130 '
140 '
150 '  INPUT VARIABLE LIST
160 '
170 '  GAS MASS FLOW................
180 '  PA(in-Hg)-atmospheric pressure
190 '  TA(F)-atmospheric temperature
200 '  T24(F)-orifice inlet gas temperature
210 '  DP(in-H20)-differential orifice pressure
220 '  P1(in-H20)-orificeinlet gas pressure/below
                 atmospheric
230 '
240 '  VAPOR MASS FLOW............
250 '  WI(-)-inlet humidity ratio
260 '  WO(-)-outlet humidity ratio
270 '  MG(kg/kg-mole)-dry gas molecular weight
280 '
290 '  MASS BALANCE...............
300 '  MLI(kg/sec)-inlet water mass flow          MLO-outlet
310 '
320 '  ENERGY BALANCE.............
330 '  TGI(F)-inlet gas temperature                 TGO-outlet
340 '  TLI(F)-inlet liquid temperature              TLO-outlet
350 '
360 '  HEAT TRANSFER..............
370 '  TI(F)-internal fluid bulk temperature
380 '  TSI(F)-internal surface temperature
390 '  TSO(F)-external surface temperature
400 '  TCP(F)-internal gas temperature;for specific heat
       determination
410 '
```

```
420 PRINT
430 PRINT "IMPOSED OSCILLATION ? - YES(Z1=0)-NO(Z1=1)"
440 INPUT "Z1              :",Z1
450 PRINT
460 PRINT "GAS FLOW VARIABLES"
470 INPUT "PA,TA,T24       :",PA,TA,T24
480 INPUT "DP,P1           :",DP,P1
490 INPUT "TGI,TGO         :",TGI,TGO
500 INPUT "TLI,TLO         :",TLI,TLO
510 PRINT "VAPOR FLOW VARIABLES"
520 INPUT "WI,WO,MG        :",WI,WO,MG
530 PRINT "MASS BALANCE VARIABLES"
540 INPUT "MLI,MLO         :",MLI,MLO
550 PRINT
560 PRINT "DO YOU WANT A HEAT LOSS ANALYSIS ? - YES(W1=0)-
    NO(W1=1)"
570 INPUT "W1          :",W1
580 PRINT
590 IF W1<.1 THEN 600 ELSE 730
600 PRINT "HEAT TRANSFER VARIABLES"
610 FOR I=1 TO 9
620 PRINT
630 PRINT "I=";I
640 INPUT "TI,TSI,TSO      :",TI(I),TSI(I),TSO(I)
650 NEXT I
660 PRINT
670 PRINT "SPECIFIC HEAT DATA"
680 FOR I=1 TO 5
690 PRINT
700 PRINT "I-CP=";I
710 INPUT "TCP             :",TCP(I)
720 NEXT I
730 PRINT
740 PRINT "TO OUTPUT RESISTANCES AND H.T.-YES(X1=0)-
    NO(X1=1)"
750 PRINT "TO OUTPUT GAS PROPERTIES ETC. -YES(Y1=0)-
    NO(Y1=1)"
760 INPUT "X1,Y1           :",X1,Y1
770 GOSUB 5470
780 GOSUB 930
790 GOSUB 1160
800 GOSUB 1610
810 GOSUB 1720
820 IF W1<.1 THEN 830 ELSE 860
830 GOSUB 2220
840 GOSUB 3790
850 GOSUB 6760
860 GOSUB 6970
870 IF X1<.1 THEN 880 ELSE 890
880 GOSUB 6550
890 IF Y1<.1 THEN 900 ELSE 910
900 GOSUB 5680
910 END
```

```
920 '
930 ' SUBROUTINE TO CONVERT INPUT DATA UNITS
940 '......Conversion Factors
950 ' 3.3715 kPa/in-Hg @ 294 K
960 ' .2484  kPa/in-H2O@ 294 K
970 ' 1.8 R/K
980 '
990  PA=3.3715*PA
1000  DP=.2484*DP
1010  P1=.2484*P1
1020 TA=(TA+459.67)/1.8
1030  T24=(T24+459.67)/1.8
1040 TGI=(TGI+459.67)/1.8
1050  TGO=(TGO+459.67)/1.8
1060 TLI=(TLI+459.67)/1.8
1070  TLO=(TLO+459.67)/1.8
1080 FOR I=1 TO 9
1090 TI(I)=(TI(I)+459.67)/1.8
1100 TSI(I)=(TSI(I)+459.67)/1.8
1110  TSO(I)=(TSO(I)+459.67)/1.8
1120 TCP(I)=(TCP(I)+459.67)/1.8
1130 NEXT I
1140 RETURN
1150 '
1160 ' SUBROUTINE TO CALCULATE GAS MASS FLOW RATE
1170 '   B-diameter ratio   DENS(kg/s)-gas density P24,T24
1180 '   Y-expansion factor K-flow coefficient
1190 '   MFA(kg/s)-gas mass flow rate  RE-Reynolds number
1200 '   D1 (m) -pipe diameter   D2(m) -orifice diameter
1210 '   D1I(in)-pipe diameter   D2I(in)-orifice diameter
1220 '   M(kg/kg-mole)-total gas molecular weight
1230 '   P24(kPa)-orifice inlet gas pressure
1240 '
1250  D1=.07899
1260  D2=.025959
1270 B=D2/D1
1280 P24=PA-P1
1290  M=(1+WI)/((WI/18.016)+(1/MG))
1300 DENS=P24*M/(8.31434*T24)
1310 WGAS=WI
1320 TGAS=T24
1330 GOSUB 4280
1340 U24=UT
1350 K24=KT
1360  Y=1-(.41+.35*(B^4))*((DP/P24)/K24)
1370 MFA=1!
1380 RE1=(1.2732*MFA)/(U24*D2)
1390 ' CALCULATE FLOW COEFFICIENT...K
1400 D1I=3.11
1410 D2I=1.002
1420 A=D2I*(830-5000*B+9000*B^2-4200*B^3+530/SQR(D1I))
1430 KE1=(.364+.076/SQR(D1I))*(B^4)
1440 IF B>(.07+.5/D1I) THEN KE2=0:GOTO 1460
```

```
1450 KE2=.4*((1.6-1/D1I)^5)*(((.07+.5/D1I)-B)^2.5)
1460 IF B>.5 THEN KE3=0:GOTO 1480
1470 KE3=-(8.999999E-03+.034/D1I)*((.5-B)^1.5)
1480 IF B<.7 THEN KE4=0:GOTO 1500
1490 KE4=(65/(D1I^2)+3)*(B-.7)^2.5
1500 KE=.5993+.007/D1I+KE1+KE2+KE3+KE4
1510 KO=KE*(D2I*10^6)/(D2I*10^6+(15*A))
1520 RE1=(1.2732*MFA)/(U24*D2)
1530 K=KO*(1+A/RE1)
1540 MFA=35.124*K*Y*D2^2*SQR(DENS*DP)
1550 RE2=(1.2732*MFA)/(U24*D2)
1560 IF ABS(RE2-RE1)<25 THEN 1580
1570 GOTO 1380
1580 RETURN
1590 '
1600 '
1610 ' SUBROUTINE TO CALCULATE VAPOR FLOW RATES
1620 '  MVI(kg/s)-inlet vapor flow rate   MVO-outlet
1630 '
1640 '  Inlet Vapor Flow
1650 MVI=WI*MFA/(1+WI)
1660 '
1670 '  Outlet Vapor Flow
1680 MVO=WO*MFA/(1+WI)
1690 RETURN
1700 '
1710 '
1720 'SUBROUTINE TO CALCULATE DCHX EFFECTIVENESS AND
1730 'MASS AND ENERGY BALANCES
1740 'Q1(kW)-enthalpy change
        DM(kg/s)-liquid mass balance
1750 '   HAI(kJ/kg)-gas inlet enthalpy   HAO-outlet
1760 '   HVI(kJ/kg)- vapor   "      "    HVO-  "
1770 '   HLI(kJ/kg)-liquid   "      "    HLO-"
1780 '   CRI(-)-inlet thermal capacitence  CRO-  "
1790 '   WS(-)-saturation humidity ratio at outlet
            gas temperature
1800 '   DTLM(K)-log mean temperature difference
1810 '   NTU(-)-number of transfer units
1820 '   EFF1(-)-sensible effectiveness
1830 '   EFF2(-)-latent effectiveness
1840 '
1850 '
1860 '
1870 ' Mass Balance
1880 DM=(MVO+MLO)-(MVI+MLI)
1890 MAVG=(MLO+MLI+MVO+MVI)/2
1900 DDM=100*DM/MAVG
1910 ' Energy Balance
1920 TGH=TGI
1930 GOSUB 3930
1940 HAI=HA:HVI=HV
1950 TGH=TLI
```

```
1960 GOSUB 3930
1970 HLI=HL
1980 TGH=TGO
1990 GOSUB 3930
2000 HAO=HA:HVO=HV
2010 TGH=TLO
2020 GOSUB 3930
2030 HLO=HL
2040 Q1=(MLO*HLO+MVO*HVO+MFA/(1+WI)*HAO)-
                          (MLI*HLI+MVI*HVI+MFA/(1+WI)*HAI)
2050 ' Effectiveness Calculations
2060 TGC=TGI
2070 GOSUB 5120
2080 CPI=CPT
2090 CRI=(MLI*4.19)/(MFA*CPI)
2100 CRO=(MLO*4.18)/(MFA*CPI)
2110 EFF1=CRO*(TLO-TLI)/(TGI-TLI)
2120 GOSUB 5370
2130 WS=(18.02/MG)*PV/(PA-PV)
2140 IF WI<WS THEN 2150 ELSE 2160
2150 WS=WI
2160 QFG=HF*MFA*(WI-WS)/(1+WI)
2170 QFAC=QFG/(MFA*CPI*(TGI-TLI))
2180 EFF2=EFF1/(1+QFAC)
2190 DTLM=((TGI-TLO)-(TGO-TLI))/LOG((TGI-TLO)/(TGO-TLI))
2200 NTU1=EFF1*(TGI-TLI)/DTLM
2210 RETURN
2220 ' SUBROUTINE TO CALCULATE INTERNAL, WALL
       AND EXTERNAL HEAT TRANSFER
2230 GOSUB 2290
2240 GOSUB 2420
2250 GOSUB 2900
2260 GOSUB 3020
2270 GOSUB 3530
2280 RETURN
2290 ' SUBROUTINE TO READ SECTIONAL DATA
2300 '      RCD(K/W)-section conduction thermal resistance
2310 '      L(m)-        "    length
2320 '      DO(m)-       "    outside diameter
2330 '      E(-)-        "    material emissivity
2340 '
2350 FOR I=1 TO 9
2360 READ RCD(I),L(I),DO(I),E(I)
2370 NEXT I
2380DATA 4.54,.32,.282,.95,2.58,.23,.566,.95,6.23,
         .071,.848,.95
2390DATA 3.14,.071,.848,.95,4.71,.37,.244,.8,.27,
         .71,.0891,.95
2400 DATA 3.41,.605,.272,.8,.033,.96,.153,.95,1.28,
         .48,.333,.95
2410 RETURN
2420 ' SUBROUTINE TO CALCULATE INTERNAL CONVECTIVE
       HEAT TRANSFER
```

```
2430 '            DTI(K)-internal temperature difference
2440 '            TMI(K)-mean internal temperature
2450 '            UI(kg/m-s)-internal abs. visc.
                  K(-)-internal sp. heat ratio
2460 '            KI(W/m-K)-internal therm. cond.
                  PRI(-)-internal Prandtl no.
2470 '           REI(-)-internal Reynold's no.
                  NUI(-)-internal Nusselt no.
2480 '           RI(K/W)-internal convective thermal resist.
2490 '           QI(kW)- internal heat transfer
2500 '           DI(m)-internal section diameter
2510 '
2520 QIN=0
2530 FOR I=1 TO 9
2540 DTI(I)=TI(I)-TSI(I)
2550 TMI(I)=(TI(I)+TSI(I))/2
2560 TGAS=TMI(I)
2570 WGAS=WO
2580 GOSUB 4280
2590 UI(I)=UT
2600 KI(I)=KIT
2610 PRI(I)=PRIT
2620 ' Read sectional inside diameter and wall thickness
2630 READ DI(I),TH(I)
2640 IF I=<4 THEN 2660 ELSE 2700
2650 ' Gas inlet/liquid outlet manifold
2660 NUI(I)=DI(I)/TH(I)
2670 RI(I)=TH(I)/(KI(I)*3.1416*DI(I)*L(I))
2680 GOTO 2840
2690 ' Test section
2700 REI(I)=(1.2732*MFA)/(DI(I)*UI(I))
2710 XD(5)=2.91:XD(6)=14.79:XD(7)=13.93:XD(8)=18:XD(9)=13.08
2720 RPI(I)=(REI(I)*PRI(I)/XD(I))
2730 IF I=6 OR I=8 THEN 2740 ELSE 2820
2740 IF I=6 THEN 2760 ELSE 2790
2750 ' Turbulent entry region
2760 NUI(I)=.027*REI(I)^.8*PRI(I)^.3
2770 GOTO 2830
2780 ' Laminar entry region; q=const.
2790 NUI(I)=4.36+((.1*RPI(I))/(1+.016*RPI(I)^.8))
2800 GOTO 2830
2810 ' Laminar entry region; T=const.
2820 NUI(I)=3.66+((.104*RPI(I))/(1+.016*(RPI(I))^.8))
2830 RI(I)=1/(3.1416*NUI(I)*KI(I)*L(I))
2840 QI(I)=DTI(I)/(RI(I)*1000)
2850 IF I=9 GOTO 2870
2860 QIN=QIN+QI(I)
2870 NEXT I
2880 DATA .111,.083,.302,.146,.641,.076,.641,.076,.093,
        ,.073,,.113,,.152,,.26,
2890 RETURN
2900  ' SUBROUTINE TO CALCULATE WALL CONDUCTION
        HEAT TRANSFER
```

```
2910 '            DTW(K)-wall temperature difference
2920 '            QWALL(kW)-wall heat transfer
2930 '
2940 QWALL=0
2950 FOR I=1 TO 9
2960 DTW(I)=TSI(I)-TSO(I)
2970 QWALL(I)=DTW(I)/(RCD(I)*1000)
2980 IF I=9 GOTO 3000
2990 QWALL=QWALL+QWALL(I)
3000 NEXT I
3010 RETURN
3020 ' SUBROUTINE TO FIND EXTERNAL HEAT TRANSFER
3030 '            G(M/M^2)-grav. accelleration
                   BC(W/M^2-K^4)-Boltzmann const.
3040 '            AO(m^2)-section external surface area
3050 '            DTO(K)-external temperature difference
3060 '            TFO(K)-   "     mean fluid temperature
3070 ' ......External Dimensionless Parameters (-)
3080 ' GR-Grashof no.  RA-Rayleigh no.
       PR-Prandtl no.  NUO-Nusselt no.
3090 '  Z-zeta; measure of cylinder/flat plate variation
3100 '  FF-corrects NUO for cylinder curvature
3110 ' ......External Thermal Resistances (K/W)
3120 ' RCV-convection   RRAD-radiation
       ROUT-total parallel resistance
3130 ' ......External Heat Transfer (kW)
3140 ' QC-convection    QR-  radiation   RO-  total
3150 '
3160 G=9.802
3170 BC=5.67E-08
3180 QOUT=0
3190 QC=0
3200 QR=0
3210 FOR I=1 TO 9
3220 AO(I)=3.1416*DO(I)*L(I)
3230 TFO(I)=(TSO(I)+TA)/2
3240 DTO(I)=TSO(I)-TA
3250 TAIR=TFO(I)
3260 GOSUB 4880
3270 G1(I)=(G*DTO(I))/(TFO(I)*V(I)^2)
3280 GR(I)=G1(I)*L(I)^3
3290 RA(I)=PR(I)*GR(I)
3300 IF I=3 THEN FF(I)=1:GOTO 3380
3310 IF I=4 THEN FF(I)=1:GOTO 3400
3320 ' Vertical flat plate natural convection
3330 NUO(I)=.479*(DO(I)/L(I))*GR(I)^(1/4)
3340 Z(I)=(5.66/DO(I))*(L(I)/G1(I))^(1/4)
3350 FF(I)=1+Z(I)*.159
3360 GOTO 3410
3370 ' Horizontal flat plate natural convection
3380 IF RA(I)<1E+07 THEN NUO(I)=.54*RA(I)^.25:GOTO 3410
3390 IF RA(I)>=1E+07 THEN NUO(I)=.15*RA(I)^(1/3):GOTO 3410
3400 NUO(I)=.27*RA(I)^.25
```

```
3410 RCV(I)=FF(I)/(3.1416*DO(I)*K(I)*NUO(I))
3420 QC(I)=DTO(I)/(RCV(I)*1000)
3430 RRAD(I)=1/(BC*E(I)*AO(I)*(TSO(I)^2+TA^2)*(TSO(I)+TA))
3440 QR(I)=DTO(I)/(RRAD(I)*1000)
3450 ROUT(I)=(RRAD(I)*RCV(I))/(RRAD(I)+RCV(I))
3460 QO(I)=DTO(I)/(ROUT(I)*1000)
3470 IF I=9 GOTO 3510
3480 QOUT=QOUT+QO(I)
3490 QC=QC+QC(I)
3500 QR=QR+QR(I)
3510 NEXT I
3520 RETURN
3530 ' SUBROUTINE TO CALCULATE HEAT TRANSFER BY
       SPECIFIC HEAT
3540 '            CP(kJ/kg-K)-gas specific heat
3550 '            QCP(kW)-heat transfer from
                          fluid stream section
3560 '            QC..(kW)-total heat transfer
                           from sections 5-8
3570 FOR I=1 TO 5
3580 TGC=TCP(I)
3590 GOSUB 5120
3600 CP(I)=CPT
3610 NEXT I
3620 CP1=(CP(1)+CP(2))/2
3630 QCP(5)=MFA*CP1*(TCP(1)-TCP(2))
3640 CP2=(CP(2)+CP(3))/2
3650 QCP(6)=MFA*CP2*(TCP(2)-TCP(3))
3660 CP3=(CP(3)+CP(4))/2
3670 QCP(7)=MFA*CP3*(TCP(3)-TCP(4))
3680 CP4=(CP(4)+CP(5))/2
3690 QCP(8)=MFA*CP4*(TCP(4)-TCP(5))
3700 CP5=(CP(1)+CP(5))/2
3710 QCP5=MFA*CP5*(TCP(1)-TCP(5))
3720 QCIN=0:QCWA=0:QCO=0
3730 FOR I=5 TO 8
3740 QCIN=QCIN+QI(I)
3750 QCWA=QCWA+QWALL(I)
3760 QCO=QCO+QO(I)
3770 NEXT I
3780 RETURN
3790 ' SUBROUTINE TO CALCULATE RTOTAL, QTOTAL AND QCTOT
        (SEC. 5-9)
3800 ' This is an energy balance for the
       test section only
3810 QTOTAL=0
3820 FOR I=1 TO 9
3830 RTOTAL(I)=RCD(I)+ROUT(I)
3840 QTOTAL(I)=(TSI(I)-TA)/(RTOTAL(I)*1000)
3850 IF I=9 GOTO 3870
3860 QTOTAL=QTOTAL+QTOTAL(I)
3870 NEXT I
3880 QCTOT=0
```

```
3890 FOR I=5 TO 8
3900 QCTOT=QCTOT+QTOTAL(I)
3910 NEXT I
3920 RETURN
3930 ' SUBROUTINE TO CALCULATE GAS,
     VAPOR AND LIQUID ENTHALPY
3940 '          TGH(K)-dummy gas enthalpy temperature
3950 '          FAC(-)-interpolation factor
3960 ' ......Dummy Enthalpies (kJ/kg)
3970 ' HA-gas     HV-vapor     HL-liquid
3980 '
3990 IF TGH<303.15 THEN 4000 ELSE 4050
4000 FAC=(TGH-273.15)/30
4010 HA=FAC*29.6
4020 HV=FAC*55+2501.3
4030 HL=FAC*125.79
4040 GOTO 4270
4050 IF TGH<333.15 THEN 4060 ELSE 4110
4060 FAC=(TGH-303.15)/30
4070 HA=FAC*30.16+29.6
4080 HV=FAC*53.3+2556.3
4090 HL=FAC*125.34+125.79
4100 GOTO 4270
4110 IF TGH<363.15 THEN 4120 ELSE 4170
4120 FAC=(TGH-333.15)/30
4130 HA=FAC*30.24+59.76
4140 HV=FAC*50.5+2609.6
4150 HL=FAC*125.79+251.13
4160 GOTO 4270
4170 IF TGH<393.15 THEN 4180 ELSE 4230
4180 FAC=(TGH-363.15)/30
4190 HA=FAC*30.3+90
4200 HV=FAC*46.2+2660.1
4210 HL=FAC*126.79+376.92
4220 GOTO 4270
4230 FAC=(TGH-393.15)/30
4240 HA=FAC*30.4+120.3
4250 HV=FAC*40.2+2706.3
4260 HL=FAC*128.49+503.71
4270 RETURN
4280 ' SUBROUTINE TO CALCULATE GAS ABS. VISCOSITY,
4290 ' SP. HEAT RATIO, THERMAL CONDUCTIVITY AND PRANDTL NO.
4300 '          TGAS(K)-dummy gas temperature
4310 '          FAC(-)-interpolation factor
4320 ' ......Dummy Abs. Visc. (kg/m-s)
4330 ' UG-gas   UV-vapor   UT-mixture
4340 ' ......Dummy sp. heat ratio (-)
4350 ' KG-gas   KV-vapor   KT-mixture
4360 ' ......Dummy Internal Thermal Conductivity (W/m-K)
4370 ' KIG-gas  KIV-vapor  KIT-mixture
4380 ' ......Dummy Internal Prandtl No. (-)
4390 ' PRIG-gas PRIV-vapor PRIT-mixture
4400 '
```

```
4410 IF TGAS<300 THEN 4420 ELSE 4520
4420 FAC=(TGAS-275)/25
4430 UG=FAC*1.25E-06+1.721E-05
4440 UV=FAC*.000001+8.09E-06
4450 KG=1.401-FAC*.0008
4460 KV=1.3301-FAC*.0009
4470 KIG=FAC*.002+.0243
4480 KIV=FAC*.0013+.0183
4490 PRIG=.7135-FAC*.0065
4500 PRIV=FAC*.04+.817
4510 GOTO 4830
4520 IF TGAS < 350 THEN 4530 ELSE 4630
4530 FAC=(TGAS-300)/50
4540 UG=FAC*2.36E-06+1.846E-05
4550 UV=FAC*.000002+9.09E-06
4560 KG=1.4002-FAC*.0018
4570 KV=1.3292-FAC*.0034
4580 KIG=FAC*.0037+.0263
4590 KIV=FAC*.0034+.0196
4600 PRIG=.707-FAC*.007
4610 PRIV=FAC*.085+.857
4620 GOTO 4830
4630 IF TGAS<400 THEN 4640 ELSE 4740
4640 FAC=(TGAS-350)/50
4650 UG=FAC*2.19E-06+2.082E-05
4660 UV=FAC*1.96E-06+1.109E-05
4670 KG=1.3984-FAC*.0032
4680 KV=1.3258-FAC*.005
4690 KIG=FAC*.0038+.03
4700 KIV=FAC*.0042+.023
4710 PRIG=.7-FAC*.01
4720 PRIV=FAC*.091+.942
4730 GOTO 4830
4740 FAC=(TGAS-400)/50
4750 UG=FAC*2.06E-06+2.301E-05
4760 UV=FAC*.0000018+1.305E-05
4770 KG=1.3952-FAC*.0042
4780 KV=1.3208-FAC*.0054
4790 KIG=FAC*.0035+.0338
4800 KIV=FAC*.0059+.0272
4810 PRIG=.69-FAC*.004
4820 PRIV=FAC*.107+1.033
4830 UT=UG/(1+WI)+WGAS*UV/(1+WGAS)
4840 KT=KG/(1+WI)+WGAS*KV/(1+WGAS)
4850 KIT=KIG/(1+WI)+WGAS*KIV/(1+WGAS)
4860 PRIT=PRIG/(1+WI)+WGAS*PRIV/(1+WGAS)
4870 RETURN
4880 ' SUBROUTINE TO CALCULATE EXTERNAL FLUID PROPERTIES
4890 '            TAIR(K)-dummy external air temperature
4900 '            FAC(-)-interpolation factor
4910 '            K(W/m-K)-external thermal conductivity
4920 '            V(m^2/s)-     "      kinematic viscosity
4930 '            PT(-)-        "      Prandtl no.
```

```
4940 '
4950 IF TAIR<300 THEN 4960 ELSE 5010
4960 FAC=(TAIR-250)/50
4970 K(I)=FAC*.004+.0223
4980 V(I)=FAC*4.45E-06+1.144E-05
4990 PR(I)=.72-FAC*.013
5000 GOTO 5110
5010 IF TAIR<350 THEN 5020 ELSE 5070
5020 FAC=(TAIR-300)/50
5030 K(I)=FAC*.0037+.0263
5040 V(I)=FAC*5.03E-06+1.589E-05
5050 PR(I)=.707-FAC*.007
5060 GOTO 5110
5070 FAC=(TAIR-350)/50
5080 K(I)=FAC*.0038+.03
5090 V(I)=FAC*5.49E-06+2.092E-05
5100 PR(I)=.7-FAC*.01
5110 RETURN
5120 ' SUBROUTINE TO CALCULATE GAS SPECIFIC HEAT
5130 '          FAC(-)-interpolation factor
5140 '          CPG(kJ/kg-K)-dummy gas specific heat
5150 '          CPV(kJ/kg-K)-dummy vapor   "      "
5160 '          CPT(kJ/kg-K)-dummy total   "      "
5170 IF TGC<300 THEN 5180 ELSE 5220
5180 FAC=(TGC-273.15)/26.85
5190 CPG=FAC*.0005+1.0065
5200 CPV=FAC*.018+1.854
5210 GOTO 5350
5220 IF TGC<350 THEN 5230 ELSE 5270
5230 FAC=(TGC-300)/50
5240 CPG=FAC*.002+1.007
5250 CPV=FAC*.082+1.872
5260 GOTO 5350
5270 IF TGC<400 THEN 5280 ELSE 5320
5280 FAC=(TGC-350)/50
5290 CPG=FAC*.005+1.009
5300 CPV=FAC*.204+1.954
5310 GOTO 5350
5320 FAC=(TGC-400)/50
5330 CPG=FAC*.007+1.014
5340 CPV=FAC*.402+2.56
5350 CPT=CPG/(1+WI)+(WI/(1+WI))*CPV
5360 RETURN
5370 ' SUBROUTINE TO CALCULATE SATURATION PRESSURE AND
5380 ' AND HEAT OF VAPORIZATION
5390 '           PV(kPa)-  saturation pressure @ TLI
5400 '           HF(kJ/kg)-heat of vaporization @ TLI
5410 IF TLI<283.15 THEN 5420 ELSE 5440
5420 PV=1.017+.21*(TLI-280.37)/2.78
5430 GOTO 5450
5440 PV=1.227+.54*(TLI-283.15)/5.56
5450 HF=2491-14*(TLI-280.37)/8.34
5460 RETURN
```

```
5470 ' SUBROUTINE TO EXAMINE INPUT DATA
5480  LPRINT  ".............INPUT  DATA................."
5490 LPRINT
5500 LPRINT "PA(in-Hg) TA(F) T24(F) DP(in-H20) P1(in-H20)"
5510 LPRINT PA,TA,T24,DP,P1
5520 LPRINT
5530 LPRINT " TGI(F)     TGO(F)     TLI(F)     TLO(F)"
5540 LPRINT TGI,TGO,TLI,TLO
5550 LPRINT
5560 LPRINT " WI            WO            MG"
5570 LPRINT WI,WO,MG
5580 LPRINT
5590 LPRINT " MLI(kg/s)     MLO(kg/s)"
5600 LPRINT MLI,MLO
5610 LPRINT
5620 IF W1<.1 THEN 5630 ELSE 5670
5630 LPRINT " I       TI(F)    TSI(F)   TSO(F)   TCP(F)"
5640 FOR I=1 TO 9
5650 LPRINT I,TI(I),TSI(I),TSO(I),TCP(I)
5660 NEXT I
5670 RETURN
5680 ' SUBROUTINE TO OUTPUT-CONVERTED INPUT, ENTHALPIES.
5690 ' SECTION DATA, GAS PROPERTIES,N/D PARAMETERS AND
5700 '  EXTERNAL THERMAL RESISTANCE AND HEAT TRANSFER
5710 LPRINT
5720 LPRINT "*****************************************"
5730 LPRINT "*****************************************"
5740 LPRINT
5750 GOSUB 5470
5760 GOSUB 5800
5770 GOSUB 5910
5780 GOSUB 6010
5790 RETURN
5800 ' SUBROUTINE TO OUTPUT GAS,VAPOR AND LIQUID ENTHALPIES
5810 LPRINT
5820 LPRINT
5830 LPRINT "....GAS,VAPOR AND LIQUID ENTHALPIES...."
5840 LPRINT
5850 LPRINT " HAI(kJ/kg)    HVI(kJ/kg)    HLI(kJ/kg)"
5860 LPRINT HAI,HVI,HLI
5870 LPRINT
5880 LPRINT " HAO(kJ/kg)    HVO(kJ/kg)    HLO(kJ/kg)"
5890 LPRINT HAO,HVO,HLO
5900 RETURN
5910 ' SECTION DATA SUBROUTINE
5920 LPRINT
5930 LPRINT
5940  LPRINT  ".............SECTION  DATA................"
5950 LPRINT
5960 LPRINT " I        RCD(K/W)    L(m)      DO(m)     E"
5970 FOR I=1 TO 9
5980 LPRINT I,RCD(I),L(I),DO(I),E(I)
5990 NEXT I
```

```
6000 RETURN
6010 ' GAS PROPERTIES AND N/D VALUES OUTPUT SUBROUTINE
6020 LPRINT
6030 LPRINT
6040 LPRINT ".........INTERNAL GAS PROPERTIES..........."
6050 LPRINT
6060 LPRINT " I     TMI(K)  UI(kg/m-s)  KI(W/m-K)  PRI(-)"
6070 FOR I=1 TO 9
6080 LPRINT I,TMI(I),UI(I),KI(I),PRI(I)
6090 NEXT I
6100 LPRINT
6110 LPRINT
6120 LPRINT ".......EXTERNAL AIR PROPERTIES........."
6130 LPRINT
6140 LPRINT " I     TFO(K)    K(W/m-K)   V(m^2/s)   PR(-)"
6150 FOR I=1 TO 9
6160 LPRINT I,TFO(I),K(I),V(I),PR(I)
6170 NEXT I
6180 LPRINT
6190 LPRINT
6200 LPRINT "......NON-DIMENSIONAL PARAMETERS....."
6210 LPRINT
6220 LPRINT " I        GR(-)     NUO(-)    REI(-)    NUI(-)"
6230 FOR I=1 TO 9
6240 LPRINT I,GR(I),NUO(I),REI(I),NUI(I)
6250 NEXT I
6260 LPRINT
6270 LPRINT
6280 LPRINT ".........GAS SPECIFIC HEATS........."
6290 LPRINT
6300 LPRINT "CP1(kJ/kg-K)=",CP1
6310 LPRINT "CP2(kJ/kg-K)=",CP2
6320 LPRINT "CP3(kJ/kg-K)=",CP3
6330 LPRINT "CP4(kJ/kg-K)=",CP4
6340 LPRINT "CP5(KJ/KG-K)=",CP5
6350 RETURN
6360 ' SUBROUTINE TO OUTPUT EXTERNAL THERMAL RESISTANCE AND
     HEAT TRANFER"
6370 LPRINT
6380 LPRINT "****************************************"
6390 LPRINT
6400 LPRINT "......EXTERNAL THERMAL RESISTANCE....."
6410 LPRINT
6420 LPRINT " I        RCV(K/W)    RRAD(K/W)   ROUT(K/W)"
6430 FOR I=1 TO 9
6440 LPRINT I,RCV(I),RRAD(I),ROUT(I)
6450 NEXT I
6460 LPRINT
6470 LPRINT
6480 LPRINT ".........EXTERNAL HEAT TRANSFER..........."
6490 LPRINT
6500 LPRINT " I        QCV(kW)      QRAD(kW)     QOUT(kW)"
6510 FOR I=1 TO 9
```

```
6520 LPRINT I,QC(I),QR(I),QO(I)
6530 NEXT I
6540 RETURN
6550 ' SUBROUTINE TO OUTPUT RADIAL AND EXTERNAL THERMAL
       RESISTANCE AND H.T.
6560 GOSUB 6360
6570 GOSUB 6590
6580 RETURN
6590 ' SUBROUTINE TO OUTPUT RADIAL THERMAL RESISTANCE AND
       HEAT TRANSFER
6600 LPRINT
6610 LPRINT
6620 LPRINT ".........RADIAL THERMAL RESISTANCE........."
6630 LPRINT
6640 LPRINT"I   RIN(K/W)   RWALL(K/W)   ROUT(K/W)   RTOT(K/W)"
6650 FOR I=1 TO 9
6660 LPRINT I,RI(I),RCD(I),ROUT(I),RTOTAL(I)
6670 NEXT I
6680 LPRINT
6690 LPRINT ".........RADIAL HEAT TRANSFER............"
6700 LPRINT
6710 LPRINT "I   QIN(kW)   QWALL(kW)   QOUT(kW)   QTOT(kW)"
6720 FOR I=1 TO 9
6730 LPRINT I,QI(I),QWALL(I),QO(I),QTOTAL(I)
6740 NEXT I
6750 RETURN
6760 ' SUBROUTINE TO OUTPUT ENERGY BALANCE FOR
       SECTIONS 5-8
6770 LPRINT
6780 LPRINT "*******************************************"
6790 LPRINT
6800 LPRINT"...PARTIAL ENERGY BALANCE-SECTIONS(SEC.5-8).."
6810 LPRINT
6820 LPRINT"QIN(kW)   QWALL(kW)   QOUT(kW)   QTOT(kW)   QCP(kW)"
6830 LPRINT
6840 FOR I=5 TO 8
6850 LPRINT QI(I),QWALL(I),QO(I),QTOTAL(I),QCP(I)
6860 NEXT I
6870 LPRINT
6880 LPRINT
6890 LPRINT".......PARTIAL ENERGY BALANCE SUM(SEC.5-8)....."
6900 LPRINT
6910 LPRINT "QIN(kW)=",QCIN
6920 LPRINT "QWAL(kW)=",QCWA
6930 LPRINT "QOUT(kW)=",QCO
6940 LPRINT "QTOT(kW)=",QCTOT
6950 LPRINT "QCP(kW)=",QCP5
6960 RETURN
6970 ' SUBROUTINE TO OUTPUT MASS FLOW, MASS AND
       ENERGY BALANCE
6980 ' AND EFFECTIVENESS RESULTS
6990 LPRINT
7000 LPRINT "*******************************************"
```

```
7010 LPRINT
7020 LPRINT ".............MASS FLOW DATA................."
7030 LPRINT
7040 IF Z1<.1 THEN 7050 ELSE 7070
7050 LPRINT "SHAKING"
7060 GOTO 7080
7070 LPRINT "NOT SHAKING"
7080 LPRINT
7090 LPRINT "MFA(kg/s)=",MFA
7100 LPRINT "TGI(K)=",TGI
7110 LPRINT "MLI(KG/S)=",MLI
7120 LPRINT "CRI(-)=",CRI
7130 LPRINT "WS(kg/kg)=",WS
7140 LPRINT
7150 LPRINT ".........MASS AND ENERGY BALANCE............"
7160 LPRINT
7170 LPRINT "DMAS(%)=",DDM
7180 LG=100*(1-MLO/MLI)
7190 LPRINT "MLI(kg/s)=",MLI
7200 LPRINT "MLO(kg/s)=",MLI
7210 LPRINT "MVI(kg/s)=",MVI
7220 LPRINT "MVO(kg/s)=",MVO
7230 LPRINT "MLOST(kg/s)=",DM
7240 LPRINT "MBAL(%)=",DDM
7250 LPRINT "LIQUID GAIN(%)=",LG
7260 IF W1<.1 THEN 7270 ELSE 7350
7270 LPRINT "DENERGY(kW)=",Q1
7280 LPRINT
7290 LPRINT "...........TOTAL HEAT LOSS................."
7300 LPRINT
7310 LPRINT "QIN(kW)=",QIN
7320 LPRINT "QWALL(kW)=",QWALL
7330 LPRINT "QOUT(kW)=",QOUT
7340 LPRINT "QTOTAL(kW)=",QTOTAL
7350 LPRINT
7360 LPRINT "..........H2O ENERGY GAIN DATA..............."
7370 LPRINT
7380 LPRINT "EFF1(-)=",EFF1
7390 LPRINT
7400 LPRINT "EFF2(-)=",EFF2
7410 LPRINT
7420 LPRINT "NTU1(-)=",NTU1
7430 LPRINT
7440 RETURN
```

Izbicki, Stephen F.
Latent heat recovery
from a counterflow...

DATE	ISSUED TO